Energy Reports 8 (2022) 9805–9827

Contents lists available at ScienceDirect

Energy Reports

journal homepage: www.elsevier.com/locate/egyr

Research paper

Mitigating mismatch power loss of series–parallel and total-cross-tied array configurations using novel enhanced heterogeneous hunger games search optimizer

Dalia Yousri [a,b,1], Ehab F. El-Saadany [a,1], Yomna Shaker [b,c,1], Thanikanti Sudhakar Babu [d,1], Ahmed F. Zobaa [e,*,1], Dalia Allam [b,1]

[a] Advanced Power and Energy Center, APEC, Khalifa University, Abu Dhabi, United Arab Emirates
[b] Electrical Engineering Dept., Faculty of Engineering, Fayoum University, Fayoum, Egypt
[c] Engineering Department, University of Science and Technology of Fujairah (USTF), Fujirah, United Arab of Emirates
[d] Department of Electrical and Electronics Engineering, Chaitanya Bharathi Institute of Technology (CBIT), Hyderabad, 500075, India
[e] College of Engineering, Design & Physical Sciences, Brunel University London, Uxbridge UB8 3PH, UK

ARTICLE INFO

Article history:
Received 9 April 2022
Received in revised form 1 July 2022
Accepted 24 July 2022
Available online xxxx

Keywords:
Photovoltaic reconfiguration
Partial shading
Hunger games search
Series–parallel PV
Total-cross-tied array

ABSTRACT

The location of shaded or faulty Photovoltaic modules in the PV array has a negative impact on the harvested power from the entire array. To overcome this significant limitation, PV reconfiguration is a considerable technique developed via interchanging the PV modules' location physically or electrically. By this inspiration, in this article, the authors propose a novel enhanced heterogeneous hunger games search optimizer (EHHGS) based PV reconfiguration. The innovated EHHGS introduces a modified variant for the basic hunger game search optimizer (HGS) to achieve a high diversity and robust exploitation of the optimal solutions. The EHHGS is applied to identify the optimal relocation for the shaded or faulty modules in two configurations of PV connected array: total-cross-tied array (TCT) and Series–parallel one (S–P). The proposed approach has applied symmetric and asymmetric connected PV arrays with dimensions of 9×9 and 10×8 throughout five different shade patterns. Moreover, for providing a flexible tool for the user/researcher to detect and observe the benefits achieved via the PV reconfiguration strategy, a simple graphical user interface (GUI) for the PV reconfiguration strategy of TCT or S–P PV connected array using meta-heuristic algorithms is designed. This implemented GUI can extend for any size of PV arrays, different optimization algorithms, and different connection schemes. The proposed EHHGS, HGS, and set of recent optimizers, including harris hawk optimizer (HHO), marine predators algorithm (MPA), and artificial ecosystem-based optimization (AEO), handle a new simplified objective function to boost the optimizer's ability in catching the optimal modules' location to alleviate the mismatched power in the studied arrays. Several statistical metrics are computed for providing an unbiased comparison. Through the comparisons, the proposed EHHGS exhibits superior performance. It achieves the best re-design for the considered arrays that helps in avoiding the mismatch losses in the cases of the partial shaded/faulty modules and enhances the power generated profiles. EHHGS enhances the power by percentages of 44.42%, 11.9%, 33.36%, 20. 86% and 13.17% compared to the TCT-connected system. In the case of the S–P connection, the proposed EHHGS generates 47.2% and 10.45%, 30.75%, 17.25%, and 26.27% higher power.

© 2022 The Author(s). Published by Elsevier Ltd. This is an open access article under the CC BY license (http://creativecommons.org/licenses/by/4.0/).

1. Introduction

With the advancement of the economy, electrical energy consumption is rising day by day. However, the conventional power from gas and oil is impractical, and their utilization would contaminate the environment. Solar energy, as a reasonably sustainable asset, its application has quickly evolved nowadays (Lowe and Drummond, 2022; Yousri et al., 2020c), and it is treated as an extremely promising renewable energy resource. Nevertheless, a PV module's performance entirely relies on surrounding conditions like irradiation and temperature. In addition, some of the PV modules in a PV array may receive different levels of irradiation due to building shadows, moving clouds, snowfall, or dust formed on PV modules (Malathy and Ramaprabha, 2018). The occurrence

* Corresponding author.
E-mail address: Ahmed.Zobaa@brunel.ac.uk (A.F. Zobaa).
[1] All the authors have the same contribution.

https://doi.org/10.1016/j.egyr.2022.07.153
2352-4847/© 2022 The Author(s). Published by Elsevier Ltd. This is an open access article under the CC BY license (http://creativecommons.org/licenses/by/4.0/).

Nomenclature

Acronyms

AEO	artificial ecosystem-based optimization
EHHGS	Enhanced Heterogeneous Hunger Games2Search Optimizer
HGS	Hunger games search optimizer
HHO	harris hawk optimizer
MPA	marine predators algorithm
PSC	partial shading condition
S–P	Scheme of Series–parallel.
TCT	Scheme of Total-cross-tied

Constants

E_{gap}	Band-gap energy
K_b	Boltzmann's constant
q	Electrons charge

Variables

G_f	Actual irradiation received by each module
G_{SOC}	Irradiation at SOC
I_{array}	Total Current of a PV array
I_{mp}	Current at MPP
I_{out}	Total current generated by TDM
I_{pv}	Photo generated current
I_{string}	Total Current of a PV string
N_{ss} and N_{pp}	Number of series and parallel connected cells
P_{array}	Total power produced by PV array
R_p and R_s	parallel and series resistance
T	Absolute temperature in °C
V_{array}	Total Voltage of a PV array
V_{mp}	Voltage at MPP
V_{oc}	Voltage at open circuit
V_{string}	Total Voltage of a PV string
V_t	Thermal voltage
V_{Mo_i}, and I_{Mo_i}	Total voltage and current at row number i
V	Total voltage generated of the PV cell

of receiving different levels of irradiation is called partial shading condition (PSC). The adverse impact of PSC is cataloged as (a) hotspot formation causes permanent damage to PV modules (b) numerous peaks on the power–voltage (P–V) curve may create additional stress on the tracking of the MPP, and (c) prone to significant power loss (Mehedi et al., 2021). In addition, centralized PV power systems suffer from the mismatch among PV modules which can cause power loss, along with numerous peaks in the P–V curve (Trindade et al., 2016). Therefore, numerous researchers have attained high priority to find a suitable solution to downplay the effect of PSC. One of the best approaches is rearranging the PV module's electrical connections in a PV array (Premkumar et al., 2020). This methodology is known as PV array reconfiguration.

Reconfiguration is the technique that intends to disseminate the shade among the PV modules to form an equal row current or irradiation. The reconfiguration can be performed either through physical relocation (PR) (static) or by utilizing the electrical routing of the arrays (dynamic) (Krishna and Moger, 2021).

For the literature on static reconfiguration approaches, an odd–even reconfiguration was presented in Yadav et al. (2020) to manage the effect of partial shading under diagonally progressing shadow. Skyscraper puzzle-based technique for 6 × 6 PV array was proposed in Meerimatha and Rao (2020), the outcome of the proposed method is compared concerning conventional connection schemes and other puzzle-based technique called arrow-SuDoKu. The same Skyscraper for any type, size, and rating of a PV system was proposed in Nihanth et al. (2019). Magic square to enhance power generation is demonstrated by authors in Rakesh and Madhavaram (2016). Power comparison technique (PCT) presented in Akrami and Pourhossein (2018), enhances power generation by 11.9% than regular TCT connected system under partial shading conditions. G.Saikrishna et al. in Krishna and Moger (2019b) proposed ideal SuDoKu technique to boost the power output of TCT connected scheme. In Srinivasan et al. (2020) authors proposed a two-step reconfiguration approach to reduce the switching count of earlier methods. From the performed comparative study, via the proposed approach SuDoKu method gives superior performance to TCT (Krishna and Moger, 2019a). The other static reconfiguration techniques are Lo Shu technique (Venkateswari and Rajasekar, 2020), static shade dispersion positioning (SDP) (Satpathy and Sharma, 2018), Ken-Ken Puzzle Pattern (Murugesan et al., 2021), competence square (Dhanalakshmi and Rajasekar, 2018), fixed reconfiguration (Satpathy and Sharma, 2019). Direct power evaluation method (Zhu et al., 2020), in this, the mathematical modeling is built to obtain the maximum output power of a PV array. However, the early proposed static reconfiguration and puzzle-based techniques are one-time arrangement techniques. This may fail during the change in irradiation conditions because the shade cannot be distributed automatically. In addition, if to change the physical locations of PV modules, additional wires and much physical labor are needed. The topologies derived from SuDoKu game theory have limitations that it can be implemented where the PV array has an even number of rows. Thus, possible techniques were then proposed, by introducing power electronic switches to modify the PV module's electrical connections that are known by dynamic PV array reconfiguration techniques.

The dynamic PV array reconfiguration techniques can be categorized mainly into 3 types. In the 1st category, several approaches based on data-based algorithms were chiefly used. But these approaches involve conventional methods, namely irradiation analog compensators, and lookup tables (Faldella et al., 1991; Salameh and Dagher, 1990). These lookup table-based methods required colossal memory, and cache miss/hit continuity makes them vulnerable to switch instants. In the second category, the mathematical classic optimization algorithms were used to find the optimal switching matrix to perform reconfiguration like a branch and bound algorithm (El-Dein et al., 2012). These types of methods were not recommended as they performed the calculations with some assumptions. For the third category, other approaches were proposed based on evolutionary-based algorithms. These approaches reduced calculation burden, and high memory consumption and simplified the switching matrix generation. In addition, optimization-based algorithms were successfully employed in different engineering fields. As a result, numerous researchers were motivated to propose a solution for the impact of partial shading via an optimization-based reconfiguration approach.

Genetic algorithm-based reconfiguration was implemented for 9 × 9 PV array to equalize the current row difference (Deshkar et al., 2015). This technique required additional calculations to generate a uniform distribution matrix. In Ramasamy et al. (2016) dodging algorithm was developed for changing the switching matrix position for 3 × 3 PV array. In this technique, the PV array

was divided into the lower, middle, and upper sections to manage the switching conditions received from the switching matrix. This method was feasible in the case of high-rated PV structures as it consumes more switches. Another well-known population-based algorithm named particle swarm optimization-based reconfiguration was presented in Babu et al. (2017) to alleviate the limitations of PSC. In Alkahtani et al. (2020), time-domain reflectometry via a repositioning algorithm-based reconfiguration is proposed. Furthermore, in Ngoc et al. (2017), an iterative and hierarchical sorting method was introduced to equalize the irradiation over PV modules. Intending to implement a reconfiguration for large-scale PV arrays, authors in Yousri et al. (2020b) employed the marine predator's algorithm (MPA) to test PV array sizes of 9×9, 16×16, and 25×25. The obtained results confirm that the proposed method can be successfully used for any size of PV array system. An artificial ecosystem (AEO) based reconfiguration was implemented in Yousri et al. (2020c) for 9×9, 6×20, 16×16, and 25×25 to verify the successful reconfiguration for large size PV arrays and irrespective of symmetrical and unsymmetrical array structures. This method exhibits superior performance on robustness and reliability. High flexible reconfiguration approaches via flow regime, social mimic optimization, and Rao optimization algorithms are presented in Babu et al. (2020). Similarly, modified harris hawks optimizer (Yousri et al., 2020a) and butterfly optimization algorithm (Fathy, 2020), grasshopper optimization algorithm (GOA) (Fathy, 2018), were also implemented with the same objective of minimizing partial shading losses in a PV array systems. Further Table 1 summarizes a detailed study on various reconfiguration techniques implemented via meta-heuristic algorithms.

1.1. Research gap and novelty

From the above carried-out literature, it is understood that providing an effective methodology of PV reconfiguration for suppressing the losses with both partial shading and random failures was considered by few researchers; however, it is a highly challenging and essential issue. Moreover, few researchers proposed their approaches for reconfiguring S–P under PS because of its complexity in the implementation; however, S–P is one of the most known approaches in the PV-connected systems. Most researchers confirmed that the S–P and TCT connections are the most recommended schemes to provide the required harvested power (Ajmal et al., 2021). Thereby in this work, a novel approach is proposed for acting like a complete solution for mitigating mismatches with the partial shading and random failure losses in TCT and S–P schemes. Thus, the contributions of this work are listed as follows:

1. Proposing a novel reconfiguration technique by developing an enhanced heterogeneous hunger games search optimizer (EHHGS). The hunger games search optimizer (HGS) is selected due to its simplicity, flexibility, and less number of tunable parameters that are needed.
2. The proposed approach is implemented for reconfiguring both TCT and S–P; therefore, a novel objective function is proposed to increase the performance of the applied optimizers.
3. The reconfiguration of PV arrays with partially shaded PV modules and failed ones are considered in this work.
4. A flexible graphical user interface (GUI) for PV reconfiguration strategy of TCT or S–P PV connected array using meta-heuristic algorithms is designed. This implemented GUI can extend for any size of PV arrays, different optimization algorithms, and different connection schemes as well.
5. Two PV array sizes like 10×8 and 9×9 for TCT and S–P connected systems are evaluated using various other optimization techniques based on reconfiguration namely harris hawk optimizer (HHO), MPA, and AEO besides the basic HGS and the modified EHHGS.
6. The study is carried-out under five different shade patterns for each scheme of TCT and S–P.
7. An extensive statistical analysis is taken forward to assess the superiority of the proposed technique.

The carried-out analyses and comparisons confirm the superiority of the proposed approach in providing the optimal reconfigured patterns for the studied systems that reduces the mismatch power loss and maximize the harvested systems' power. EHHGS enhances the power by percentages of 44.42%, 11.9%, 33.36%, 20.86%, and 13.17% compared to the TCT connected system. In the case of the S–P connection, the proposed EHHGS generates 47.2% and 10.45%, 30.75%, 17.25%, and 26.27% higher power.

The article is articulated as follows: Modeling equations of considered TDM are presented in Section 2. The complete overview of system description and voltage, current, and power calculation equations of S–P and TCT schemes are given in Sections 3.1 and 3.2 respectively. The formulation of the objective function is described in Section 4. The overview, steps involved, pseudo-codes, and implementation methodology of basic and proposed EHHGS optimizer, moreover the friendly-user tool of GUI is represented in Section 5. The evaluation of the proposed methodology under different shade conditions for TCT and S–P connected systems is given in Section 6. In addition, the statistical analysis of carried-out work is given in the same section. Finally, the outcomes, observations, and superiority of the proposed reconfiguration technique are listed in Section 7.

2. Photovoltaic model : Triple diode (TDM)

Researchers are focusing on producing various types of PV modules as the use of solar PV continues to grow. SDM, DDM, and TDM are three PV models that are frequently employed. However, SDM has a disadvantage in because it lacks reliability at low irradiance levels since carrier recombination losses in the depletion area are not taken into account (Lim et al., 2015).DDM is later introduced by connecting an additional diode to SDM, which will rectify SDM's disadvantage. To deal with the effects of grain limitations and leakage current, an improved model with three diodes (TDM) is provided (Nishioka et al., 2007). In terms of achieving nonlinear behavior in PV cells, the TDM performs better than the other two models. Another significant feature of TDM is that it can be regarded as a necessary model for determining the properties of low-rated PV cells in applications (Yousri et al., 2020d). The authors used TDM to construct the PV array in this work because of its extensive features.

The electrical circuit of TDM is shown in Fig. 1. It comprises of 3 didoes D_1, D_2, and D_3, are connected in antiparallel to photo-current source, I_{pv}. R_p and R_s represents the parallel and series resistances of PV model. I_{01}, I_{02} and I_{03} defines the reverse saturation currents of 3 didoes D_1, D_2, and D_3 respectively.

The total current produced by the PV cell based on TDM may be calculated using KCL on the equivalent circuit, and it can be expressed mathematically as in Eq. (1):

$$\begin{aligned} I_{out} =& I_{pv} - I_{01}\left\{exp\left(\frac{V + I_{out}R_s}{a_1 V_t}\right) - 1\right\} \\ &- I_{02}\left\{exp\left(\frac{V + I_{out}R_s}{a_2 V_t}\right) - 1\right\} \\ &- I_{03}\left\{exp\left(\frac{V + I_{out}R_s}{a_3 V_t}\right) - 1\right\} - \frac{V + I_{out}R_s}{R_p} \end{aligned} \tag{1}$$

Table 1
Comprehensive review of various dynamic EAR reconfiguration techniques implemented so far under PSC.

Ref	Algorithm	Topology	PV array sizes	Remarks
Yousri et al. (2020c)	AEO, HHO, PSO	TCT	9×9, 6 × 20, 16 × 16, 25×25	Authors proposed new objective function for effective reconfiguration and compared with the conventional weighted objective function. Achieves consistency than PSO and HHO, also achieve around 30% of higher power than TCT.
Rezk et al. (2021)	FPA, MPA, BOA, COA	TCT	9 × 9	Evaluated under four shade patterns, enhances 26.58% of power over TCT
Nazeri et al. (2021)	FA PSC	S–P, TCT	3 × 3	Verified for 10 shade patterns, the effectiveness of the proposed method may not be recommended as since its verified under small size of PV array.
Nahidan et al. (2021)	GA		5 × 5	
Ajmal et al. (2021)	GA, PSO, MHHO	TCT	9 × 9	Verified under regular 4 shade patterns.
Varma et al. (2021)	maximum–minimum tier equalization swapping (MMTES)	TCT	3 × 3	Switching of reconfiguration takes place by equalization of tier irradiance. The examinations have been carried-out over PV simulator, thereby reliability of proposed method cant be guaranteed.
Yousri et al. (2020b)	MPA, HHO, PSO MRFO	TCT	9×9, 16 × 16, 25×25	Authors proposed a novel and innovative objective function. The proposed MPA consumes less time, and high consistency to disperse the shade.
Fathy (2020)	BOA, GWO	S–P–TCT, TCT	6 × 4	This method is of simple in implementation and construction. Requires less tunable parameters. Five shade patterns have been evaluated. Enhanced 27.43% higher power than S–P–TCT system.
Yousri et al. (2020e)	Multi-objective GWO	TCT	9 × 9	This method exhibits dynamic reconfiguration process which closes to the reality. It was verified under 6 different shade patterns. Proved it as effective in handling multiple peaks problem in P–V curves
Yousri et al. (2020a)	GA, HHO, MHHO	TCT	9×9, 6 × 4, 6×20	Proposed objective function is successfully verified for 23 standard bench mark functions. The proposed system evaluated under 12 shade patterns with experimental validation, achieved max of 33.27% of power enhancement than TCT
Babu et al. (2020)	FRA, SMO, ROA	TCT	9 × 9	FRA takes 1.5 sec for optimal structure where as GA takes 4 s Energy, revenue generation for 1 year is evaluated under real time constrains and observed that FRA technique, generates 13% higher amount of power than TCT.
Fathy (2018)	GA, GHO	TCT	9 × 9	The proposed method enhances maximum of 10% higher than regular TCT.
Babu et al. (2017)	GA, PSO	TCT	9 × 9	It achieves better performance than GA and TCT connected system, energy harvest and income generation over a period of 1 year is also evaluated for effectiveness of technique.
Deshkar et al. (2015)	GA	TCT	9 × 9	It is the first ever optimization technique implemented for reconfiguration. The superiority of GA technique is compared over GA, SuDoKu based reconfiguration methods.

where I_{pv} stands for photocurrent, $I_0 1$, $I_0 2$, and $I_0 3$ are saturation currents, V_t stands for thermal voltage constant, and it can be defined as $fracK_b * Tq$, where K_b stands for Boltzmann's constant. The symbols a_1, a_2, and a_3 stands for ideality factors of diodes.

The previous equation of Eq. (1) can be generalized as follows in Eq. (2) to express the total current and voltage of the PV module that is composed of series and parallel connected cell N_{ss} and N_{pp}, respectively.

$$I_{out} = I_{pv}N_{pp} - I_{01}N_{pp}\left\{exp\left(\frac{V + I_{out}R_s\left[\frac{N_{ss}}{N_{pp}}\right]}{a_1V_tN_{ss}}\right) - 1\right\} - I_{02}N_{pp}\left\{exp\left(\frac{V + I_{out}R_s\left[\frac{N_{ss}}{N_{pp}}\right]}{a_2V_tN_{ss}}\right) - 1\right\} - I_{03}N_{pp}\left\{exp\left(\frac{V + I_{out}R_s\left[\frac{N_{ss}}{N_{pp}}\right]}{a_3V_tN_{ss}}\right) - 1\right\} - \frac{V + I_{out}R_s\left[\frac{N_{ss}}{N_{pp}}\right]}{R_p\left[\frac{N_{ss}}{N_{pp}}\right]} \quad (2)$$

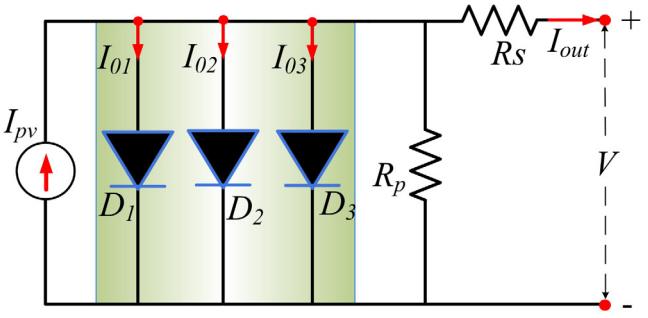

Fig. 1. Equivalent circuit of 3 diode model.

It is important to note that the parameters I_{pv}, I_{o1}, I_{o2}, I_{o3}, and R_p are all dependent terms on irradiation (G_f) or perhaps temperature (T), as shown in Eq. (3a). A condition of Eq. (3b) explains that the diodes saturation currents ($Io1, 2, 3$) are dependent on temperature, whereas the parallel resistance is dependent on G,

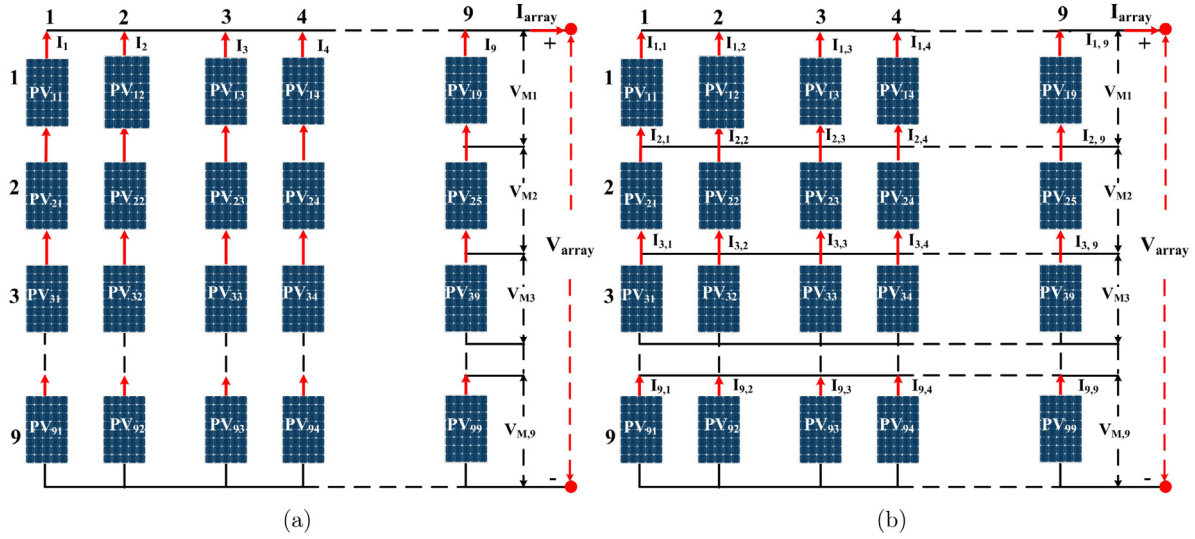

Fig. 2. Basic connections schemes, (a) Series–Parallel (S–P), and (b) Total Cross-Tied (TCT).

as shown in Eq. (3c).

$$I_{pv_{(G_f,T)}} = \left[I_{pv_{SOC}} + K_i\,(T-25)\right] \cdot \frac{G_f}{G_{SOC}} \tag{3a}$$

$$I_{o1,2,3_{(T)}} = I_{o1,2,3_{SOC}} \cdot \left(\frac{T}{T_{SOC}}\right) \cdot e^{\left(\frac{q\cdot E_g}{a_{1,2}}\right)\cdot\left(\frac{1}{T_{SOC}}-\frac{1}{T}\right)} \tag{3b}$$

$$R_{p(G)} = R_{p_{SOC}} \cdot \left(\frac{G_{SOC}}{G_f}\right) \tag{3c}$$

where $I_{pv_{SOC}}$, $I_{o1,2,3_{SOC}}$, and $R_{p_{SOC}}$ represent the produced photo current, saturation currents, and parallel resistance under standard operating conditions (SOC) of irradiation(G_{SOC} = 1000 W/m^2) and temperature ($T_{SOC} = 25°C$). The current temperature coefficient is K_i. The sign E_{gap} stands for the temperature-dependent band-gap energy, which is written as follows:

$$E_{gap} = E_{gap_{SOC}} \cdot \left[1 - 2.6677 \times 10^{-4}\,(T-25)\right] \tag{4}$$

where $E_{gap_{SOC}}$ is the band-gap energy at SOC.

3. System description

It is common knowledge that a single PV module cannot offer the required quantity of electricity; therefore, the required number of PV modules must be connected in series and parallel (S–P) to meet the energy demand. Various academics have worked on discovering new sorts of connection systems other than S–P connection to boost PV power generation in this area. Bridge link (BL), Honeycomb (HC), and Total cross-tied are the three types of connecting schemes proposed. However, the most widely used solutions rely on S–P and TCT module linkages (La Manna et al., 2014). Among the S–P and TCT connections, it is found that TCT connected system shows superior performance (Ajmal et al., 2020). The Schemes of the S–P and TCT are depicted in Fig. 2 and are detailed in the following subsections.

3.1. Series-Parallel (S–P) scheme

The S–P is the most often utilized connection in real PV power facilities. It is constructed by connecting PV modules in series to generate strings that can give the requisite voltage, and then joining these strings in parallel to enhance the overall current. Fig. 2(a) depicts the S–P setup connection diagram. With this connection scheme, the desired voltage and currents are generated. The voltage, current, and power generation of an S–P connection scheme can be derived as follows (Pachauri et al., 2019; Fang et al., 2021):

Assuming that all of the $(i \times j) = n \times m(9 \times 9)$ PV modules in Fig. 2(a) get uniform shade with a shading factor of $\frac{G_f}{G_{SOC}}$, the generated power can be expressed as (Pachauri et al., 2019; Fang et al., 2021),

$$P_{array} = \frac{G_f}{G_{SOC}} n \times m V_{Mo} I_{Mo} \tag{5}$$

where I_{Mo}, V_{Mo} are produced current and voltages under full irradiation conditions. G_{SOC} irradiation at SOC i.e., 1000 W/m^2, the $G_{f_{ij}}$ is the actual irradiation received by each module.

For the jth string : during partial shading condition as m PV modules receive less irradiation due to shade, the current of shaded PV modules are $\frac{G_{f_{ij}}}{G_{SOC}} I_{Mo}$, and other $(n-m)$ modules produces rated current I_{Mo}, n = 9 of Fig. 2(a). The current produced by series connected scheme of jth string (I_{Series_j}) is controlled by the shaded module as presented in Eq. (6) (Pachauri et al., 2019; Fang et al., 2021).

$$I_{Series_j} = I_{shaded_j} = \frac{G_{f_{ij}}}{G_{SOC}} I_{Mo} \tag{6}$$

To calculate the voltage of Fig. 2(a) during partial shading condition, there are two cases as discussed below (Pachauri et al., 2019; Fang et al., 2021) :

- Case 1: In the absence of a bypass diode, the shaded PV modules limit the string current. PV modules linked by this bypass diode stay inactive as long as the string current is less than the current of the shaded modules. In *Vstring*, the voltage across the bypass diode is largely ignored. Eq. (7) can be used to determine the *Vstring* of the jth string of Fig. 2(a).

$$V_{string_j} = \sum_{i=1}^{n} V_{Mo}. \qquad n = 9 \quad \text{of Fig. 2(a)} \tag{7}$$

- Case 2 : When the string current exceeds the current produced by the shaded PV modules, the diode bypasses the shaded PV modules. The current and voltage generated by the string are represented as following. Note, the voltage drop across the bypass diode is ignored. Pachauri et al.

(2019), Fang et al. (2021),

$$\begin{aligned} &I_{string_j} = I_{Mo} \\ &V_{string_j} = (n-m)\, V_{Mo} \qquad n = 9 \quad \text{of Fig. 2(a)} \end{aligned} \tag{8}$$

When these PV modules of cases 1, 2 are connected in parallel, the I_{array}, V_{array} and P_{array} of Fig. 2(a) are given in Eq. (9) as described below (Pachauri et al., 2019; Fang et al., 2021)

$$\begin{aligned} I_{array} &= \sum_{j=1}^{m} \frac{G_{f_{ij}}}{G_{SOC}} I_{Mo} + (n-m)\, I_{Mo} \\ &\qquad \forall i, \quad i = 1 : n = 9 \quad \text{of Fig. 2(a)} \\ V_{array} &= min\{V_{string_j}\} \qquad j = 1, 2, 3, \ldots, m, \; and \\ &\qquad \forall i, \quad i = 1 : n. \quad n, m = 9 \quad \text{of Fig. 2(a)} \\ P_{array} &= \left[\sum_{j=1}^{m} \frac{G_{f_{ij}}}{G_{SOC}} I_{Mo} + (n-m)\, I_{Mo} \right] min\{V_{string_j}\} \\ &\qquad j = 1, 2, 3, \ldots, m, \quad and \quad \forall i \end{aligned} \tag{9}$$

3.2. Total-Cross-tied (TCT) scheme

One of the other often employed connecting techniques is TCT. It is a better variant of the S–P configuration. Despite the fact that S–P and TCT module schemes produce about identical amounts of electricity under uniform conditions, in partial shade conditions, the TCT connected system outperforms the S–P (Premkumar et al., 2020). In a TCT scheme, the inclusion of cross-connections decreases mismatching losses and increases power generation. Fig. 2(b) shows the connection diagram of a 9×9 TCT linked array. Each PV module is identified as PV_{ij}, with i and j denoting the row and column numbers, respectively. The module PV_{23}, for example, describes the module's location, which is connected at the 2nd row and 3rd column. To estimate the value currently produced by each PV module, use the quantity of incoming radiation as indicated in Eq. (10) (Yousri et al., 2020c):

$$I_{ij} = \frac{G_{f_{ij}}}{G_{SOC}} I_{M_{SOC_{ij}}} \tag{10}$$

where G_{SOC} refers to the irradiation levels that received by each module at (i, j) location in the array under normal test circumstances, i.e. 1000 W/m^2, and $G_{f_{ij}}$ is the real radiation received by each module at (i, j) location in the array. The generated current by a PV module at the standard G_0 is$I_{M_{SOC_{ij}}}$, while the module current at $Gfij$ at the ith, jth row and column is I_{ij}.

By employing KCL, and KVL; the total row current value (I_{Row_i}), and the total array voltage (V_{array_j}) of each jth column in the considered TCT scheme can be evaluated as follows (Yousri et al., 2020c):

$$I_{Row_i} = \sum_{j=1}^{m} \left(\frac{G_{f_{ij}}}{G_{SOC}} I_{M_{SOC_{ij}}} \right), where \quad i = 1, 2, 3, \ldots.., n \tag{11a}$$

$$\begin{aligned} V_{array_j} &= \sum_{i=1}^{n} V_{M_i}, where \quad j = 1, 2, 3, \ldots.., m \\ &\quad n, m = 9 \quad \text{of Fig. 2(b)} \end{aligned} \tag{11b}$$

where V_{M_i} and I_{Row_i} are the total voltage and current at ith row number.

4. Implementation of the PV array reconfiguration process

To maximize the output power of S–P or TCT-connected arrays that include partially shaded or random failed PV modules, reconfiguring the locality of these modules is recognized as the recent optimal solution. The meta-heuristics optimization algorithms are a flexible and efficient strategy to provide optimal locations to the array modules. For enhancing the optimization process, an efficient objective function is required to be identified. Therefore, in this work, an innovative objective function is proposed to promote the maximization of the PV array's harvested power and achieve smoothness in the PV characteristics. The developed objective function is a maximization optimization problem for the multiplication of the difference between the maximum and minimum power levels in the array and the average power across the array. The proposed objective function can be formulated as follows:

$$Fitnessfunction = (max\{P\} - min\{P\}) * P\_aveg \tag{12}$$

where the Fitness function is the implemented objective function. The symbol P is the power vector of the array. For S–P connection the vector P is the power levels of each string as in case of Fig. 2(a), the power vector can be written as $[P_j] = [P_1, P_2, \ldots., \ldots., ..P_9]$, where 9 strings (9 columns) are connected in parallel. For TCT connection of Fig. 2(b), the vector of power P_i includes the power of each row in the array that can be formulated as $[P_i] = [P_1, P_2, \ldots., \ldots., ..P_9]$, where 9 rows are connected in series. The P_aveg is the average power value of the power vector $[P]$ that calculated as $\frac{1}{n}\sum_{i=1}^{n}[P_i]$. By inspecting the proposed objective, one can deduce that the fitness function is maximized when the P_aveg power has large values, and the difference between the maximum and minimum power levels is significant. This observation is achieved when most of the strings (columns) in the S–P or rows in TCT have the closed values to the maximum power. By this strategy, the level of the obtained maximum power is promoted, and the deviation between most of the vector values is minimized, which means achieving smoothness characteristics in the PV array.

5. Enhanced Heterogeneous Hunger Games Search Optimizer

In this part, an enhanced heterogeneous hunger games search optimizer (EHHGS) is proposed to handle the PV array reconfiguration process reliably. The structure of the proposed EHHGS is presented in detail as follows:

5.1. Basic Hunger Games Search Optimizer (HGS): Overview

The HGS is a recently created optimizer by Yang et al. (2021) to mimic the starvation-driven activities and behavioral activities of mammals. There are two types of social behavior among the mammals While looking for food; in the first behavior, the mammals collaborate as one group (team-work spirit). On the other hand, few individuals do not participate in the cooperation while they rely on their skills to find the foods (self-dependence behavior) in the second behavior. For mimicking these social behaviors, Yang et al. (2021) modeled the following formulas as core equations of the HGS.

$$S_i(\vec{t+1}) = \begin{cases} GS_1 : S_i(\vec{t}).\,(1 + randn(1)) \\ \qquad Rd_1 < F, \\ GS_2 : \vec{\gamma_{1_i}}(t).\vec{S_i^{bs}}(t) + \vec{B_i}(t).\vec{\gamma_{2_i}}(t).|\vec{S_i^{bs}}(t) - S_i(\vec{t})| \\ \qquad Rd_1 > F, Rd_2 > D(t), \\ GS_3 : \vec{\gamma_{1_i}}(t).\vec{S_i^{bs}}(t) - \vec{B_i}(t).\vec{\gamma_{2_i}}(t).|\vec{S_i^{bs}}(t) - S_i(\vec{t})| \\ \qquad Rd_1 > F, Rd_2 < D(t) \end{cases} \tag{13}$$

where $\vec{S_i^{bs}}(t)$ denotes the position of the corresponding individual to the best fitness function at iteration t, the $\vec{S_i}(t)$ refers to the location of the ith search agent. The $\vec{\gamma_1}$ and $\vec{\gamma_2}$ symbolize the levels of starvation used to produce appetite signals where $\vec{\gamma_1}$ is representing the inaccuracy in finding the correct position while $\vec{\gamma_2}$ is representing the manipulation of starvation's efficacy on the range of work. The expression of $\vec{S_i}(t).(1 + randn(1))$ of Eq. (13) depicts the hungry agent's random behavior while seeking for food at the present location (t). The term $\vec{S_i^{bs}}(t) - \vec{S_i}(t)|$ of Eq. (13) represents the range of work of the ith agent at present t. The weight $(\vec{\gamma_2})$ is multiplied in that term $(|\vec{S_i^{bs}}(t) - \vec{S_i}(t)|)$ to regulate the range of work, so the agent can cease seeking when it is no longer hungry. Adding and eliminating the expression of $\vec{\gamma_1}.\vec{S_i^{bs}}(t)$ in the second the third lines of Eq. (13) describes the present agent becoming familiar with its competition while seeking food, and then continuing to hunt for food at the present position once the food is conquered. Based on the original text of HGS (Yang et al., 2021), the F is a constant value of 0.03. The symbol $vecB$ stands for a ranging controller, which has values in the range [−b b] and is used to restrict the work interval, as a result, it is progressively reduced to 0. The Rd_1, Rd_2 are random values withdrawn from a range of [0 1] while $randn(1)$ is a randomly withdrawn number from a normal distribution. The decision-making of Eq. (13) is influenced by the variable D, which may be calculated using the following equation (Yang et al., 2021).

$$D_i(t) = sech\left(|Fit_i(t) - Fit^*(t)|\right) \qquad i \in 1, 2, 3, \ldots., N_{agent} \tag{14}$$

where Fit_i is the value of the fitness function of the ith search agent at iteration t, and Fit^* is the best fitness function achieved thus far in iteration t. The N_{agent} represents the total number of agents. The hyperbolic function equivalent to $1/Cosh(x)$ is denoted by the symbol $sech(x)$.

Again, by inspecting the core equations of HGS of Eq. (13), one can note that the 1st line of the equation is an emulation of the self-dependence behavior. In contrast, the 2nd and 3rd lines are simulations of team cooperation work. The 2nd and 3rd lines are mainly controlled by 3 variables that are $\vec{B}$, $\vec{\gamma_1}$ and $\vec{\gamma_2}$; In Yang et al. (2021) tuned the considered variables via using the given equations:

- Tuning the ranging controller $(\vec{B})$: In Yang et al. (2021) modeled the Eq. (15) to represent its shrinking behavior across the iterations (t):

$$\begin{aligned} &\vec{B_i}(t) = 2 \times Sh_i(t) \times Rd_3 - Sh_i(t), \\ &where, \\ &Sh_i(t) = 2 \times \left(1 - \frac{t}{Max_T}\right) \end{aligned} \tag{15}$$

  where Max_T is the total iteration numbers, the Rd_3 is a randomly selected number in the range of [0 1].
- Tuning the weights $(\vec{\gamma_1})$ and $(\vec{\gamma_2})$: (Yang et al., 2021) formulated the given equations to enhance the agent's behavior while searching for the foods.

$$\vec{\gamma_{1_i}}(t) = \begin{cases} Hungry_i(t).\frac{M}{Sum\_Hungry(t)} \times Rd_4 & Rd_5 < F, \\ 1 & Rd_5 > F \end{cases} \tag{16}$$

$$\vec{\gamma_{2_i}}(t) = (1 - exp\,(-|Hungry_i(t) - Sum\_Hungry(t)|)) \times Rd_6 \times 2 \tag{17}$$

  where the symbols of Rd_4, Rd_5, and Rd_6 are random numbers belong to the interval of [0 1]. The $Hungry_i(t)$ stands to the hunger ith agent while $Sum\_Hungry(t)$ is the sum of the hungry feelings of all agents at iteration (t). The representation of $Hungry_i(t)$ is formulated as below (Yang et al., 2021):

$$Hungry_i(t) = \begin{cases} 0 & Fit_i(t) == Global^*(t) \\ Hungry_i(t) + New\_Hungry_i(t) & Fit_i(t)! = Global^*(t). \end{cases} \tag{18}$$

where $New\_Hungry_i(t)$ refers to a new hunger that is added if the fitness function of the ith agent is not equal to the best-obtained fitness so far. Hence the corresponding new hunger of different agents is different. Accordingly, Yang et al. (Yang et al., 2021) gave the following mathematical formula for the new hunger (Yang et al., 2021).

$$New\_Hungry_i(t) = \begin{cases} F\_S \times (1 + Rd) & K\_S < F\_S \\ K\_S_i(t) & K\_S \geq F\_S., \end{cases}$$

$$where$$

$$K\_S_i(t) = \frac{Fit_i(t) - Global^*(t)}{Worst^*(t) - Global^*(t)} \times Rd_7 \times 2 \times (Max\_B - Min\_B) \tag{19}$$

where $Worst^*(t)$ shows the worst value of Fit achieved in iteration (t). The variables Max_B and Min_B indicates the upper and lower limits of the search area. Yang et al. advocate a constant value of 100 for the F_S (Yang et al., 2021).

5.2. Proposed Enhanced Heterogeneous Hunger Games Search Optimizer

The basic HGS algorithm structure has the limitation of falling into the local solutions. The authors considered a transfer factor F of a value of 0.03 to transmit from the self-dependence behavior into teamwork behavior. Through this tactic, the authors did not control the number of agents that followed the self-dependence behavior or the teamwork behavior, which impacted discovering the search space. Furthermore, in striking the agents in the local solutions, the agents fail to move away from this trap as there is no enhanced diversification strategy. Therefore, HGS's novel variant is proposed, called the Enhanced Heterogeneous Hunger Games Search Optimizer (EHHGS), to avoid falling into the local solutions. In EHHGS, the search agents are categorized into two heterogeneous subgroups, one for the self-dependent agents and the other for the agents that cooperate in teamwork. The two subgroups are implemented separately thus the control parameter F of the basic HGS is not employed in the HHGS variant. Moreover, the heterogeneous HGS (HHGS) is enhanced by using the non-uniform mutation operator (Wang et al., 2020) to enhance the diversity in the second group responsible for teamwork agents to discover the search space efficiently and escape from the local solutions as described in Algorithm 1.

The main frame of the proposed EHHGS is summarized in Algorithm 2. For the maximum iteration numbers Max_T, the initial set of solutions are modified as they are divided into separate heterogeneous two groups. The first group follows (Eq. (13)(1)) In contrast, the second group follows (Eq. (13)(2,3)), and the non-uniform mutation operator is employed for this subgroup to ensure the diversity of the solutions. The modification process is repeated until the termination criterion is met.

5.3. User-friendly tool: Graphical User interface (GUI)

For helping the user/researcher to observe the response of the connected S–P or TCT PV connected system before and after the reconfiguration process, a Matlab-Graphical User interface (GUI)

Algorithm 1 The non-uniform mutation operator (Wang et al., 2020)

for Each individual i ($i = g_1 + 1, ..., N_{agent}$) **do**
  for Each dimension j ($j = 1, ..., DIM$) **do**
    if rand < 0.1 **then**
      $a = rand1(1, D)$; $N_{d\times d} = diag(a)$;
      if round (rand2) = 0 **then**
        Modify the individual location via
        $$S_{ij} = S_{ij} + N_{d\times d}\left(Max\_B_j - S_{ij}\right)\left(1 - \frac{t}{Max_T}\right)^2$$
      else if round (rand3) = 1 **then**
        Modify the individual location via
        $$0S_{ij} = S_{ij} + N_{d\times d}\left(S_{ij} - Min\_B_j\right)\left(1 - \frac{t}{Max_T}\right)^2$$
      end if
    end if
  end for
end for

where rand, rand1, rand2, rand3 are randomly selected values withdrawn from the interval of [0 1]. The round is a Matlab function to approximate the value to the nearest decimal or integer; exp: round (0.55) is 1 and round (0.4) is 0.

is designed as depicted in Fig. 3 to be a flexible and efficient interface tool. Through the GUI, the user can select his designed system (S–P or TCT) and upload the shaded pattern. The user can choose the optimizer that is performed to reconfigure such of this shaded array. Once the optimizer has been performed, the array's current, voltage, and power levels, moreover the reconfigured array, are displayed as in the Tables in the middle of Fig. 3. The user can plot the characteristics of the PV array before and after the reconfiguration process to observe the modifications gained via this strategy, as shown in the curves of Fig. 3.

6. Results and discussion

The proposed EHHGS is tested on two different PV array connections in this section: total-cross-tied (TCT) and series–parallel (S–P). For each link, five shade patterns are evaluated; the studied patterns vary in their complexity of spreading shading and defective modules in the array. PV arrays of 9×9 and 10×8 dimensions are constructed in this section. In addition to the fundamental HGS, several contemporary optimizers, such as the Harris hawk optimizer (HHO), Marine Predators Algorithm (MPA), and artificial ecosystem-based optimization (AEO), are used to evaluate and demonstrate the quality and dependability of the proposed EHHGS-approach. Throughout 30 different runs, the completed algorithms are built using the same population size (50) and iteration numbers (40). All simulations and analyses are run on a laptop with a Core i7-6500U CPU, 16 GB of RAM, and a 2.5 GHz processor. EHHGS compares the applied optimizers to the equivalents using many quality criteria, including the percentage of power loss (% PL), mismatch power loss (MPL), and power enhancement (% PH) (HHO, MPA, AEO, and HGS). The measurements are calculated to demonstrate the viability in the practice of the suggested EHHGS-approach as well as the PV array power saved. The following are the formulas for the efficiency measurement factors:

- MPL (W)= $P_{Max_{IC}} - P_{GMPP_{PS}}$
- $\%PL = \frac{P_{Max_{SOC}} - P_{GMPP_{PS}}}{P_{Max_{SOC}}}$
- $\%PH = \frac{P_{GMPP_{PS_{EHHGS}}} - P_{GMPP_{PS_{other}}}}{P_{GMPP_{PS_{other}}}} \times 100$

Algorithm 2 Steps of EHHGS

Set the EHHGS parameters; N agents, number of iterations (Max_T), L, D, L_H, Sum_hunger, number of agents in group 1 ($g1$) , group 2 ($g2$)
Calculate the initial solutions matrix.
Set t=1.
while termination criteria are not met **do**
  Evaluate the objective function (Fit) for all search agents.
  Update the Best (Fit^*), Worst (W^*) values of the fitness function and assign the best solutions (S^{bs}) .
  Calculate the Hungry using Eq.(17).
  Update the weight γ_1 using Eq.(15) .
  Update the weight γ_2 using Eq.(16) .
  for The first group of the agents ($i = 1, ..., g1$) **do**
    Update the agents locations of group 1 using Eq. (13(1)).
  end for
  for The second group of the agents ($i = g1 + 1, ..., N$) **do**
    Update the agents' locations using Eq. (13(2,3)).
    Apply Algorithm 1 to implement non-uniform mutation operator for the solutions of group 2.
  end for
  Regroup the search agents.
  t=t+1.
end while
Display the best solutions
=0

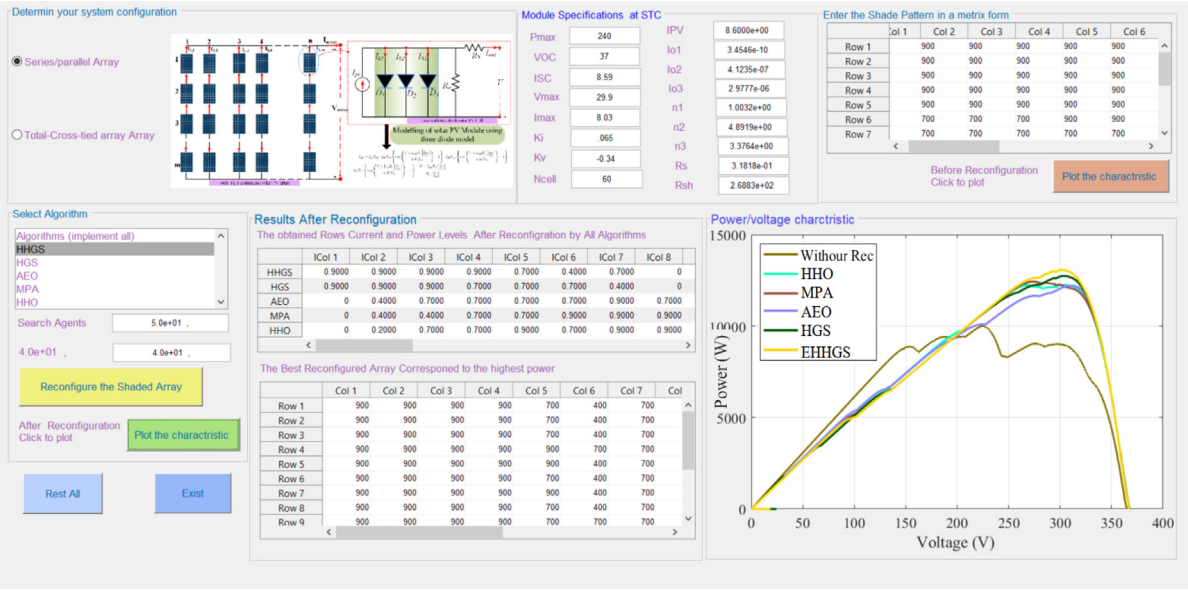

Fig. 3. Graphical-User Interface for PV reconfiguration strategy of S–P or TCT PV connected array using meta-heuristic algorithms.

Table 2
Electrical specifications of the Canadian Solar (CS6P-240P) PV module (Anon, 2003).

Parameters	Data
P_{max} (W)	240.097
V_{mp} (V)	29.9
I_{mp} (A)	8.03
V_{oc} (V)	37.0
I_{sc} (A)	8.59
N_s	60
NOCT (°C)	47
K_i (% /°C)	0.063702
K_v (% /°C)	−0.3641

The K_i, K_v are Temperature coefficients for current, and voltage, respectively.

where, the generated global power levels at the fully irradiated condition and at PS, respectively, are $P_{Max_{(IC)}}$ and $P_{GMPP_{(PS)}}$. The $P_{Max_{SOC}}$ is the global maximum power point at the standard operating condition (SOC). The $P_{GMPP_{PS_{AEO}}}$ and $P_{GMPP_{PS_{other}}}$, respectively, represent the global power obtained by the EHHGS-scheme and other approaches, which include S–P/TCT configuration, HGS, AEO, MPA, and HHO.

The electrical specification of the used PV module are listed in Table 2. With using this module, the global maximum power of a fully illuminated composed TCT/S–P arrays of dimensions 9 × 9 and 10 × 8 are 1.9420e+04 and 1.9181e+04, respectively.

6.1. Total-cross-tied (TCT) connected system discussion

This section focuses on evaluating the proposed EHHGS while handling the reconfiguration process for TCT PV arrays under five different shade patterns and accounting for random faulty modules. The first and second patterns are devoted for a 9 × 9 PV array. The array includes partially shaded and random failed modules, as depicted in Figs. 4(a), 5(a) for TCT connection without reconfiguration. For the first pattern, the array was subjected to partial shadings with a profile of (900 W/m^2, 600 W/m^2, 400 W/m^2.200 W/m^2); apart from partial shadings; four failed PV modules (located at '24', '47','82', and '89') without power generation are set. For the second pattern, the incident irradiation on the array has levels of (900 W/m^2, 700 W/m^2, 500 W/m^2. 300 W/m^2); moreover, the array in this pattern includes a four failed module in the locations of ('25', '54','68', and '82'). For the array of dimension 10 × 8, it is subjected to three different patterns (3rd, 4th, 5th) that may be known by the short-wide shading, long-narrow shading, and two-part shading, respectively as illustrated in Figs. 6(a), 7(a), and 8(a) for TCT connection without reconfiguration. The patterns of Figs. 6(a), 7(a), and 8(a) include partially shaded modules that received the irradiation with levels of partial shadings with a profile of (900 W/m^2, 700 W/m^2, 400 W/m^2.200 W/m^2) besides two failed modules that located at the third row and the eighth column ('38') and the tenth row and the second column '102'.

The reconfigured arrays based on the proposed EHHGS and other counterparts are depicted in Figs. 4, 5 and Figs. 6, 7, 8 for 9 × 9 and 10 × 8 PV arrays, respectively. The values of rows' current, voltage and power are calculated for the studied arrays in Tables 3 and 4 for the 9 × 9 and 10 × 8 PV arrays, respectively. The reported results of the tables confirm that the EHHGS discovers the most quality reconfigured patterns where the patterns-based EEHGS provides the highest harvested power of 52.2 $V_{Mo}I_{Mo}$, 57 $V_{Mo}I_{Mo}$, 57 $V_{Mo}I_{Mo}$, and 56 $V_{Mo}I_{Mo}$ for the 1st, 3rd, 4th and 5th patterns . In contrast, the EHHGS and the MPA, HGS, and AEO counterparts have the same Max_{power} of 59.4 $V_{Mo}I_{Mo}$ for pattern 2. Whereas inspecting the reported results of pattern 2 at the Table 4 shows that pattern 2 of EHHGS (see Fig. 5(f)) has the least number of peaks where the power changed in three ladder levels only of (59.4 $V_{Mo}I_{Mo}$, 34.5 $V_{Mo}I_{Mo}$, 7.1$V_{Mo}I_{Mo}$); meanwhile, the other counterparts patterns includes at least four levels. For the captured power by the MPA, AEO, HHO and HGS have the values of 51.3 $V_{Mo}I_{Mo}$, 56 $V_{Mo}I_{Mo}$, 56 $V_{Mo}I_{Mo}$, and 55 $V_{Mo}I_{Mo}$ for the 1st, 3rd, 4th and 5th patterns of 9 × 9 and 10 × 8 PV arrays, respectively as reported in Tables 3 and 4.

The Power–Voltage (P–V) and Current–Voltage (I–V) characteristics corresponded to the reconfigured patterns are plotted in Figs. 9, and 10 for 9 × 9 and 10 × 8 PV arrays, respectively. By inspecting the curves, one can detect the smoothness of the attained characteristics compared to the TCT without reconfiguration. Furthermore, the number of the local peak is diminished, and the global maximum power point (Max_{power}) is enhanced is means the rows' current levels become closely matched. The curves based on the EHHGS solution show the highest levels of the Max_{power} that confirm its efficiency and reliability.

Table 3
The TCT, HHO, MPA, AEO, HGS and EHHGS schemes' current, voltage and power values of 9 × 9 PV array.

Pattern 1

TCT scheme				HHO scheme				MPA scheme				AEO scheme				HGS scheme				EHHGS scheme			
I_i	I (A)	V (V)	P (W)	I_i	I (A)	V (V)	P (W)	I_i	I (A)	V (V)	P (W)	I_i	I (A)	V (V)	P (W)	I_i	I (A)	V (V)	P (W)	I_i	I (A)	V (V)	P (W)
I_8	2.8 I_{Mo}	9 V_{Mo}	25.2 $I_{Mo}V_{Mo}$	I_1	5.7 I_{Mo}	9 V_{Mo}	51.3 $I_{Mo}V_{Mo}$	I_3	5.7 I_{Mo}	9 V_{Mo}	51.3 $I_{Mo}V_{Mo}$	I_5	5.7 I_{Mo}	9 V_{Mo}	51.3 $I_{Mo}V_{Mo}$	I_3	5.7 I_{Mo}	9 V_{Mo}	51.3 $I_{Mo}V_{Mo}$	I_3	5.8 I_{Mo}	9 V_{Mo}	52.2 $I_{Mo}V_{Mo}$
I_7	3.6 I_{Mo}	8 V_{Mo}	28.8 $I_{Mo}V_{Mo}$	I_2	5.7 I_{Mo}	9 V_{Mo}	51.3 $I_{Mo}V_{Mo}$	I_5	5.7 I_{Mo}	9 V_{Mo}	51.3 $I_{Mo}V_{Mo}$	I_8	5.7 I_{Mo}	9 V_{Mo}	51.3 $I_{Mo}V_{Mo}$	I_5	5.7 I_{Mo}	9 V_{Mo}	51.3 $I_{Mo}V_{Mo}$	I_5	5.8 I_{Mo}	9 V_{Mo}	52.2 $I_{Mo}V_{Mo}$
I_9	3.6 I_{Mo}	8 V_{Mo}	28.8 $I_{Mo}V_{Mo}$	I_5	5.7 I_{Mo}	9 V_{Mo}	51.3 $I_{Mo}V_{Mo}$	I_6	5.7 I_{Mo}	9 V_{Mo}	51.3 $I_{Mo}V_{Mo}$	I_1	5.8 I_{Mo}	7 V_{Mo}	40.6 $I_{Mo}V_{Mo}$	I_2	5.8 I_{Mo}	7 V_{Mo}	40.6 $I_{Mo}V_{Mo}$	I_6	5.8 I_{Mo}	9 V_{Mo}	52.2 $I_{Mo}V_{Mo}$
I_6	5.2 I_{Mo}	6 V_{Mo}	31.2 $I_{Mo}V_{Mo}$	I_7	5.7 I_{Mo}	9 V_{Mo}	51.3 $I_{Mo}V_{Mo}$	I_7	5.7 I_{Mo}	9 V_{Mo}	51.3 $I_{Mo}V_{Mo}$	I_2	5.8 I_{Mo}	7 V_{Mo}	40.6 $I_{Mo}V_{Mo}$	I_4	5.8 I_{Mo}	7 V_{Mo}	40.6 $I_{Mo}V_{Mo}$	I_7	5.8 I_{Mo}	9 V_{Mo}	52.2 $I_{Mo}V_{Mo}$
I_5	6.9 I_{Mo}	5 V_{Mo}	34.5 $I_{Mo}V_{Mo}$	I_3	5.8 I_{Mo}	5 V_{Mo}	29 $I_{Mo}V_{Mo}$	I_8	5.7 I_{Mo}	9 V_{Mo}	51.3 $I_{Mo}V_{Mo}$	I_6	5.8 I_{Mo}	7 V_{Mo}	40.6 $I_{Mo}V_{Mo}$	I_7	5.8 I_{Mo}	7 V_{Mo}	40.6 $I_{Mo}V_{Mo}$	I_8	5.8 I_{Mo}	9 V_{Mo}	52.2 $I_{Mo}V_{Mo}$
I_2	7.2 I_{Mo}	4 V_{Mo}	28.8 $I_{Mo}V_{Mo}$	I_4	5.9 I_{Mo}	4 V_{Mo}	23.6 $I_{Mo}V_{Mo}$	I_9	5.9 I_{Mo}	4 V_{Mo}	23.6 $I_{Mo}V_{Mo}$	I_9	5.8 I_{Mo}	7 V_{Mo}	40.6 $I_{Mo}V_{Mo}$	I_8	5.8 I_{Mo}	7 V_{Mo}	40.6 $I_{Mo}V_{Mo}$	I_9	5.8 I_{Mo}	9 V_{Mo}	52.2 $I_{Mo}V_{Mo}$
I_4	7.2 I_{Mo}	4 V_{Mo}	28.8 $I_{Mo}V_{Mo}$	I_6	5.9 I_{Mo}	4 V_{Mo}	23.6 $I_{Mo}V_{Mo}$	I_1	6 I_{Mo}	3 V_{Mo}	18 $I_{Mo}V_{Mo}$	I_3	5.9 I_{Mo}	3 V_{Mo}	17.7 $I_{Mo}V_{Mo}$	I_1	5.9 I_{Mo}	3 V_{Mo}	17.7 $I_{Mo}V_{Mo}$	I_2	5.9 I_{Mo}	3 V_{Mo}	17.7 $I_{Mo}V_{Mo}$
I_1	8.1 I_{Mo}	2 V_{Mo}	16.2 $I_{Mo}V_{Mo}$	I_9	6.1 I_{Mo}	2 V_{Mo}	12.2 $I_{Mo}V_{Mo}$	I_4	6.1 I_{Mo}	2 V_{Mo}	12.2 $I_{Mo}V_{Mo}$	I_7	5.9 I_{Mo}	3 V_{Mo}	17.7 $I_{Mo}V_{Mo}$	I_6	5.9 I_{Mo}	3 V_{Mo}	17.7 $I_{Mo}V_{Mo}$	I_4	5.9 I_{Mo}	3 V_{Mo}	17.7 $I_{Mo}V_{Mo}$
I_3	8.1 I_{Mo}	2 V_{Mo}	16.2 $I_{Mo}V_{Mo}$	I_8	6.2 I_{Mo}	1 V_{Mo}	6.2 $I_{Mo}V_{Mo}$	I_2	6.2 I_{Mo}	1 V_{Mo}	6.2 $I_{Mo}V_{Mo}$	I_4	6.3 I_{Mo}	1 V_{Mo}	6.3 $I_{Mo}V_{Mo}$	I_9	6.3 I_{Mo}	1 V_{Mo}	6.3 $I_{Mo}V_{Mo}$	I_1	6.1 I_{Mo}	1 V_{Mo}	6.1 $I_{Mo}V_{Mo}$

Pattern 2

TCT scheme				HHO scheme				MPA scheme				AEO scheme				HGS scheme				EHHGS scheme			
I_8	5.4 I_{Mo}	9 V_{Mo}	48.6 $I_{Mo}V_{Mo}$	I_1	6.5 I_{Mo}	9 V_{Mo}	58.5 $I_{Mo}V_{Mo}$	I_1	6.6 I_{Mo}	9 V_{Mo}	59.4 $I_{Mo}V_{Mo}$	I_4	6.6 I_{Mo}	9 V_{Mo}	59.4 $I_{Mo}V_{Mo}$	I_1	6.6 I_{Mo}	9 V_{Mo}	59.4 $I_{Mo}V_{Mo}$	I_1	6.6 I_{Mo}	9 V_{Mo}	59.4 $I_{Mo}V_{Mo}$
I_7	6.3 I_{Mo}	8 V_{Mo}	50.4 $I_{Mo}V_{Mo}$	I_5	6.5 I_{Mo}	9 V_{Mo}	58.5 $I_{Mo}V_{Mo}$	I_2	6.6 I_{Mo}	9 V_{Mo}	59.4 $I_{Mo}V_{Mo}$	I_6	6.6 I_{Mo}	9 V_{Mo}	59.4 $I_{Mo}V_{Mo}$	I_3	6.6 I_{Mo}	9 V_{Mo}	59.4 $I_{Mo}V_{Mo}$	I_5	6.6 I_{Mo}	9 V_{Mo}	59.4 $I_{Mo}V_{Mo}$
I_9	6.3 I_{Mo}	8 V_{Mo}	50.4 $I_{Mo}V_{Mo}$	I_3	6.7 I_{Mo}	7 V_{Mo}	46.9 $I_{Mo}V_{Mo}$	I_4	6.6 I_{Mo}	9 V_{Mo}	59.4 $I_{Mo}V_{Mo}$	I_7	6.6 I_{Mo}	9 V_{Mo}	59.4 $I_{Mo}V_{Mo}$	I_4	6.6 I_{Mo}	9 V_{Mo}	59.4 $I_{Mo}V_{Mo}$	I_6	6.6 I_{Mo}	9 V_{Mo}	59.4 $I_{Mo}V_{Mo}$
I_5	6.4 I_{Mo}	6 V_{Mo}	38.4 $I_{Mo}V_{Mo}$	I_4	6.8 I_{Mo}	6 V_{Mo}	40.8 $I_{Mo}V_{Mo}$	I_5	6.6 I_{Mo}	9 V_{Mo}	59.4 $I_{Mo}V_{Mo}$	I_8	6.6 I_{Mo}	9 V_{Mo}	59.4 $I_{Mo}V_{Mo}$	I_5	6.7 I_{Mo}	6 V_{Mo}	40.2 $I_{Mo}V_{Mo}$	I_8	6.6 I_{Mo}	9 V_{Mo}	59.4 $I_{Mo}V_{Mo}$
I_2	6.8 I_{Mo}	5 V_{Mo}	34 $I_{Mo}V_{Mo}$	I_6	6.8 I_{Mo}	6 V_{Mo}	40.8 $I_{Mo}V_{Mo}$	I_7	6.7 I_{Mo}	5 V_{Mo}	33.5 $I_{Mo}V_{Mo}$	I_3	6.7 I_{Mo}	5 V_{Mo}	33.5 $I_{Mo}V_{Mo}$	I_2	6.8 I_{Mo}	5 V_{Mo}	34 $I_{Mo}V_{Mo}$	I_2	6.9 I_{Mo}	5 V_{Mo}	34.5 $I_{Mo}V_{Mo}$
I_6	6.8 I_{Mo}	5 V_{Mo}	34 $I_{Mo}V_{Mo}$	I_7	6.8 I_{Mo}	6 V_{Mo}	40.8 $I_{Mo}V_{Mo}$	I_6	6.9 I_{Mo}	4 V_{Mo}	27.6 $I_{Mo}V_{Mo}$	I_5	6.7 I_{Mo}	5 V_{Mo}	33.5 $I_{Mo}V_{Mo}$	I_7	6.9 I_{Mo}	4 V_{Mo}	27.6 $I_{Mo}V_{Mo}$	I_3	6.9 I_{Mo}	5 V_{Mo}	34.5 $I_{Mo}V_{Mo}$
I_4	7.3 I_{Mo}	3 V_{Mo}	21.9 $I_{Mo}V_{Mo}$	I_9	6.8 I_{Mo}	6 V_{Mo}	40.8 $I_{Mo}V_{Mo}$	I_8	6.9 I_{Mo}	4 V_{Mo}	27.6 $I_{Mo}V_{Mo}$	I_2	6.9 I_{Mo}	3 V_{Mo}	20.7 $I_{Mo}V_{Mo}$	I_8	6.9 I_{Mo}	4 V_{Mo}	27.6 $I_{Mo}V_{Mo}$	I_7	6.9 I_{Mo}	5 V_{Mo}	34.5 $I_{Mo}V_{Mo}$
I_3	7.7 I_{Mo}	2 V_{Mo}	15.4 $I_{Mo}V_{Mo}$	I_2	6.9 I_{Mo}	2 V_{Mo}	13.8 $I_{Mo}V_{Mo}$	I_9	6.9 I_{Mo}	4 V_{Mo}	27.6 $I_{Mo}V_{Mo}$	I_1	7.1 I_{Mo}	2 V_{Mo}	14.2 $I_{Mo}V_{Mo}$	I_9	6.9 I_{Mo}	4 V_{Mo}	27.6 $I_{Mo}V_{Mo}$	I_9	6.9 I_{Mo}	5 V_{Mo}	34.5 $I_{Mo}V_{Mo}$
I_1	8.1 I_{Mo}	1 V_{Mo}	8.1 $I_{Mo}V_{Mo}$	I_8	7.3 I_{Mo}	1 V_{Mo}	7.3 $I_{Mo}V_{Mo}$	I_3	7.3 I_{Mo}	1 V_{Mo}	7.3 $I_{Mo}V_{Mo}$	I_9	7.3 I_{Mo}	1 V_{Mo}	7.3 $I_{Mo}V_{Mo}$	I_6	7.1 I_{Mo}	1 V_{Mo}	7.1 $I_{Mo}V_{Mo}$	I_4	7.1 I_{Mo}	1 V_{Mo}	7.1 $I_{Mo}V_{Mo}$

Where I_i is the ith row current, I_{Mo} is the module current at SOC.

Table 4
The TCT, HHO, MPA, AEO, HGS and EHHGS schemes' current, voltage and power values of 10 × 8 PV array.

Pattern 3

TCT scheme				HHO scheme				MPA scheme				AEO scheme				HGS scheme				EHHGS scheme			
I_i	I (A)	V (V)	P (W)	I_i	I (A)	V (V)	P (W)	I_i	I (A)	V (V)	P (W)												
I_{10}	3 I_{Mo}	10 V_{Mo}	30 $I_{Mo}V_{Mo}$	I_3	5.6 I_{Mo}	10 V_{Mo}	56 $I_{Mo}V_{Mo}$	I_1	5.6 I_{Mo}	10 V_{Mo}	56 $I_{Mo}V_{Mo}$	I_1	5.6 I_{Mo}	10 V_{Mo}	56 $I_{Mo}V_{Mo}$	I_1	5.6 I_{Mo}	10 V_{Mo}	56 $I_{Mo}V_{Mo}$	I_1	5.7 I_{Mo}	10 V_{Mo}	57 $I_{Mo}V_{Mo}$
I_9	3.7 I_{Mo}	9 V_{Mo}	33.3 $I_{Mo}V_{Mo}$	I_4	5.6 I_{Mo}	10 V_{Mo}	56 $I_{Mo}V_{Mo}$	I_4	5.6 I_{Mo}	10 V_{Mo}	56 $I_{Mo}V_{Mo}$	I_4	5.6 I_{Mo}	10 V_{Mo}	56 $I_{Mo}V_{Mo}$	I_2	5.6 I_{Mo}	10 V_{Mo}	56 $I_{Mo}V_{Mo}$	I_3	5.7 I_{Mo}	10 V_{Mo}	57 $I_{Mo}V_{Mo}$
I_8	4.1 I_{Mo}	8 V_{Mo}	32.8 $I_{Mo}V_{Mo}$	I_5	5.6 I_{Mo}	10 V_{Mo}	56 $I_{Mo}V_{Mo}$	I_5	5.6 I_{Mo}	10 V_{Mo}	56 $I_{Mo}V_{Mo}$	I_5	5.6 I_{Mo}	10 V_{Mo}	56 $I_{Mo}V_{Mo}$	I_6	5.6 I_{Mo}	10 V_{Mo}	56 $I_{Mo}V_{Mo}$	I_4	5.7 I_{Mo}	10 V_{Mo}	57 $I_{Mo}V_{Mo}$
I_7	5.6 I_{Mo}	7 V_{Mo}	39.2 $I_{Mo}V_{Mo}$	I_6	5.6 I_{Mo}	10 V_{Mo}	56 $I_{Mo}V_{Mo}$	I_8	5.6 I_{Mo}	10 V_{Mo}	56 $I_{Mo}V_{Mo}$	I_6	5.6 I_{Mo}	10 V_{Mo}	56 $I_{Mo}V_{Mo}$	I_8	5.6 I_{Mo}	10 V_{Mo}	56 $I_{Mo}V_{Mo}$	I_5	5.7 I_{Mo}	10 V_{Mo}	57 $I_{Mo}V_{Mo}$
I_3	6.3 I_{Mo}	6 V_{Mo}	37.8 $I_{Mo}V_{Mo}$	I_7	5.6 I_{Mo}	10 V_{Mo}	56 $I_{Mo}V_{Mo}$	I_9	5.6 I_{Mo}	10 V_{Mo}	56 $I_{Mo}V_{Mo}$	I_9	5.6 I_{Mo}	10 V_{Mo}	56 $I_{Mo}V_{Mo}$	I_9	5.6 I_{Mo}	10 V_{Mo}	56 $I_{Mo}V_{Mo}$	I_8	5.7 I_{Mo}	10 V_{Mo}	57 $I_{Mo}V_{Mo}$
I_6	6.4 I_{Mo}	5 V_{Mo}	32 $I_{Mo}V_{Mo}$	I_8	5.6 I_{Mo}	10 V_{Mo}	56 $I_{Mo}V_{Mo}$	I_{10}	5.6 I_{Mo}	10 V_{Mo}	56 $I_{Mo}V_{Mo}$	I_{10}	5.6 I_{Mo}	10 V_{Mo}	56 $I_{Mo}V_{Mo}$	I_{10}	5.6 I_{Mo}	10 V_{Mo}	56 $I_{Mo}V_{Mo}$	I_9	5.7 I_{Mo}	10 V_{Mo}	57 $I_{Mo}V_{Mo}$
I_1	7.2 I_{Mo}	4 V_{Mo}	28.8 $I_{Mo}V_{Mo}$	I_2	5.8 I_{Mo}	4 V_{Mo}	23.2 $I_{Mo}V_{Mo}$	I_6	5.9 I_{Mo}	4 V_{Mo}	23.6 $I_{Mo}V_{Mo}$	I_2	5.8 I_{Mo}	4 V_{Mo}	23.2 $I_{Mo}V_{Mo}$	I_4	5.8 I_{Mo}	4 V_{Mo}	23.2 $I_{Mo}V_{Mo}$	I_2	5.8 I_{Mo}	4 V_{Mo}	23.2 $I_{Mo}V_{Mo}$
I_2	7.2 I_{Mo}	4 V_{Mo}	28.8 $I_{Mo}V_{Mo}$	I_9	5.8 I_{Mo}	4 V_{Mo}	23.2 $I_{Mo}V_{Mo}$	I_3	6 I_{Mo}	3 V_{Mo}	18 $I_{Mo}V_{Mo}$	I_8	5.9 I_{Mo}	3 V_{Mo}	17.7 $I_{Mo}V_{Mo}$	I_5	5.8 I_{Mo}	4 V_{Mo}	23.2 $I_{Mo}V_{Mo}$	I_6	5.8 I_{Mo}	4 V_{Mo}	23.2 $I_{Mo}V_{Mo}$
I_4	7.2 I_{Mo}	4 V_{Mo}	28.8 $I_{Mo}V_{Mo}$	I_1	5.9 I_{Mo}	2 V_{Mo}	11.8 $I_{Mo}V_{Mo}$	I_7	6.1 I_{Mo}	2 V_{Mo}	12.2 $I_{Mo}V_{Mo}$	I_7	6.1 I_{Mo}	2 V_{Mo}	12.2 $I_{Mo}V_{Mo}$	I_3	6.3 I_{Mo}	2 V_{Mo}	12.6 $I_{Mo}V_{Mo}$	I_{10}	5.8 I_{Mo}	4 V_{Mo}	23.2 $I_{Mo}V_{Mo}$
I_5	7.2 I_{Mo}	4 V_{Mo}	28.8 $I_{Mo}V_{Mo}$	I_{10}	6.8 I_{Mo}	1 V_{Mo}	6.8 $I_{Mo}V_{Mo}$	I_2	6.3 I_{Mo}	1 V_{Mo}	6.3 $I_{Mo}V_{Mo}$	I_3	6.5 I_{Mo}	1 V_{Mo}	6.5 $I_{Mo}V_{Mo}$	I_7	6.4 I_{Mo}	1 V_{Mo}	6.4 $I_{Mo}V_{Mo}$	I_7	6.3 I_{Mo}	1 V_{Mo}	6.3 $I_{Mo}V_{Mo}$

Pattern 4

TCT scheme				HHO scheme				MPA scheme				AEO scheme				HGS scheme				EHHGS scheme			
I_i	I (A)	V (V)	P (W)	I_i	I (A)	V (V)	P (W)	I_i	I (A)	V (V)	P (W)												
I_{10}	3.9 I_{Mo}	10 V_{Mo}	39 $I_{Mo}V_{Mo}$	I_4	5.6 I_{Mo}	10 V_{Mo}	56 $I_{Mo}V_{Mo}$	I_1	5.6 I_{Mo}	10 V_{Mo}	56 $I_{Mo}V_{Mo}$	I_1	5.6 I_{Mo}	10 V_{Mo}	56 $I_{Mo}V_{Mo}$	I_1	5.6 I_{Mo}	10 V_{Mo}	56 $I_{Mo}V_{Mo}$	I_1	5.7 I_{Mo}	10 V_{Mo}	57 $I_{Mo}V_{Mo}$
I_9	4.8 I_{Mo}	9 V_{Mo}	43.2 $I_{Mo}V_{Mo}$	I_9	5.6 I_{Mo}	10 V_{Mo}	56 $I_{Mo}V_{Mo}$	I_2	5.8 I_{Mo}	9 V_{Mo}	52.2 $I_{Mo}V_{Mo}$	I_2	5.6 I_{Mo}	10 V_{Mo}	56 $I_{Mo}V_{Mo}$	I_2	5.6 I_{Mo}	10 V_{Mo}	56 $I_{Mo}V_{Mo}$	I_9	5.7 I_{Mo}	10 V_{Mo}	57 $I_{Mo}V_{Mo}$
I_8	5 I_{Mo}	8 V_{Mo}	40 $I_{Mo}V_{Mo}$	I_{10}	5.6 I_{Mo}	10 V_{Mo}	56 $I_{Mo}V_{Mo}$	I_3	5.8 I_{Mo}	9 V_{Mo}	52.2 $I_{Mo}V_{Mo}$	I_3	5.6 I_{Mo}	10 V_{Mo}	56 $I_{Mo}V_{Mo}$	I_3	5.8 I_{Mo}	8 V_{Mo}	46.4 $I_{Mo}V_{Mo}$	I_2	5.8 I_{Mo}	8 V_{Mo}	46.4 $I_{Mo}V_{Mo}$
I_7	5.3 I_{Mo}	7 V_{Mo}	37.1 $I_{Mo}V_{Mo}$	I_1	5.8 I_{Mo}	7 V_{Mo}	40.6 $I_{Mo}V_{Mo}$	I_4	5.8 I_{Mo}	9 V_{Mo}	52.2 $I_{Mo}V_{Mo}$	I_4	5.6 I_{Mo}	10 V_{Mo}	56 $I_{Mo}V_{Mo}$	I_4	5.8 I_{Mo}	8 V_{Mo}	46.4 $I_{Mo}V_{Mo}$	I_3	5.8 I_{Mo}	8 V_{Mo}	46.4 $I_{Mo}V_{Mo}$
I_6	5.8 I_{Mo}	6 V_{Mo}	34.8 $I_{Mo}V_{Mo}$	I_2	5.8 I_{Mo}	7 V_{Mo}	40.6 $I_{Mo}V_{Mo}$	I_5	5.8 I_{Mo}	9 V_{Mo}	52.2 $I_{Mo}V_{Mo}$	I_5	5.6 I_{Mo}	10 V_{Mo}	56 $I_{Mo}V_{Mo}$	I_6	5.8 I_{Mo}	8 V_{Mo}	46.4 $I_{Mo}V_{Mo}$	I_5	5.8 I_{Mo}	8 V_{Mo}	46.4 $I_{Mo}V_{Mo}$
I_3	6.1 I_{Mo}	5 V_{Mo}	30.5 $I_{Mo}V_{Mo}$	I_3	5.8 I_{Mo}	7 V_{Mo}	40.6 $I_{Mo}V_{Mo}$	I_6	5.8 I_{Mo}	9 V_{Mo}	52.2 $I_{Mo}V_{Mo}$	I_8	5.6 I_{Mo}	10 V_{Mo}	56 $I_{Mo}V_{Mo}$	I_7	5.8 I_{Mo}	8 V_{Mo}	46.4 $I_{Mo}V_{Mo}$	I_6	5.8 I_{Mo}	8 V_{Mo}	46.4 $I_{Mo}V_{Mo}$
I_4	6.6 I_{Mo}	4 V_{Mo}	26.4 $I_{Mo}V_{Mo}$	I_6	5.8 I_{Mo}	7 V_{Mo}	40.6 $I_{Mo}V_{Mo}$	I_7	5.8 I_{Mo}	9 V_{Mo}	52.2 $I_{Mo}V_{Mo}$	I_{10}	5.6 I_{Mo}	10 V_{Mo}	56 $I_{Mo}V_{Mo}$	I_8	5.8 I_{Mo}	8 V_{Mo}	46.4 $I_{Mo}V_{Mo}$	I_7	5.8 I_{Mo}	8 V_{Mo}	46.4 $I_{Mo}V_{Mo}$
I_5	6.6 I_{Mo}	4 V_{Mo}	26.4 $I_{Mo}V_{Mo}$	I_7	5.8 I_{Mo}	7 V_{Mo}	40.6 $I_{Mo}V_{Mo}$	I_8	5.8 I_{Mo}	9 V_{Mo}	52.2 $I_{Mo}V_{Mo}$	I_7	5.7 I_{Mo}	3 V_{Mo}	17.1 $I_{Mo}V_{Mo}$	I_9	5.8 I_{Mo}	8 V_{Mo}	46.4 $I_{Mo}V_{Mo}$	I_8	5.8 I_{Mo}	8 V_{Mo}	46.4 $I_{Mo}V_{Mo}$
I_2	6.8 I_{Mo}	2 V_{Mo}	13.6 $I_{Mo}V_{Mo}$	I_8	5.8 I_{Mo}	7 V_{Mo}	40.6 $I_{Mo}V_{Mo}$	I_9	5.8 I_{Mo}	9 V_{Mo}	52.2 $I_{Mo}V_{Mo}$	I_6	6 I_{Mo}	2 V_{Mo}	12 $I_{Mo}V_{Mo}$	I_{10}	5.8 I_{Mo}	8 V_{Mo}	46.4 $I_{Mo}V_{Mo}$	I_{10}	5.8 I_{Mo}	8 V_{Mo}	46.4 $I_{Mo}V_{Mo}$
I_1	7 I_{Mo}	1 V_{Mo}	7 $I_{Mo}V_{Mo}$	I_5	6.3 I_{Mo}	1 V_{Mo}	6.3 $I_{Mo}V_{Mo}$	I_{10}	5.9 I_{Mo}	1 V_{Mo}	5.9 $I_{Mo}V_{Mo}$	I_9	7 I_{Mo}	1 V_{Mo}	7 $I_{Mo}V_{Mo}$	I_5	6.1 I_{Mo}	1 V_{Mo}	6.1 $I_{Mo}V_{Mo}$	I_4	5.9 I_{Mo}	1 V_{Mo}	5.9 $I_{Mo}V_{Mo}$

Pattern 5

TCT scheme				HHO scheme				MPA scheme				AEO scheme				HGS scheme				EHHGS scheme			
I_i	I (A)	V (V)	P (W)	I_i	I (A)	V (V)	P (W)	I_i	I (A)	V (V)	P (W)												
I_8	4.6 I_{Mo}	10 V_{Mo}	46 $I_{Mo}V_{Mo}$	I_1	5.5 I_{Mo}	10 V_{Mo}	55 $I_{Mo}V_{Mo}$	I_1	5.5 I_{Mo}	10 V_{Mo}	55 $I_{Mo}V_{Mo}$	I_5	5.5 I_{Mo}	10 V_{Mo}	55 $I_{Mo}V_{Mo}$	I_2	5.5 I_{Mo}	10 V_{Mo}	55 $I_{Mo}V_{Mo}$	I_2	5.6 I_{Mo}	10 V_{Mo}	56 $I_{Mo}V_{Mo}$
I_7	4.8 I_{Mo}	9 V_{Mo}	43.2 $I_{Mo}V_{Mo}$	I_2	5.5 I_{Mo}	10 V_{Mo}	55 $I_{Mo}V_{Mo}$	I_2	5.5 I_{Mo}	10 V_{Mo}	55 $I_{Mo}V_{Mo}$	I_8	5.5 I_{Mo}	10 V_{Mo}	55 $I_{Mo}V_{Mo}$	I_{10}	5.5 I_{Mo}	10 V_{Mo}	55 $I_{Mo}V_{Mo}$	I_5	5.7 I_{Mo}	9 V_{Mo}	51.3 $I_{Mo}V_{Mo}$
I_9	5 I_{Mo}	8 V_{Mo}	40 $I_{Mo}V_{Mo}$	I_5	5.6 I_{Mo}	8 V_{Mo}	44.8 $I_{Mo}V_{Mo}$	I_6	5.5 I_{Mo}	10 V_{Mo}	55 $I_{Mo}V_{Mo}$	I_2	5.6 I_{Mo}	8 V_{Mo}	44.8 $I_{Mo}V_{Mo}$	I_6	5.6 I_{Mo}	8 V_{Mo}	44.8 $I_{Mo}V_{Mo}$	I_1	5.8 I_{Mo}	8 V_{Mo}	46.4 $I_{Mo}V_{Mo}$
I_6	5.3 I_{Mo}	7 V_{Mo}	37.1 $I_{Mo}V_{Mo}$	I_6	5.6 I_{Mo}	8 V_{Mo}	44.8 $I_{Mo}V_{Mo}$	I_9	5.5 I_{Mo}	10 V_{Mo}	55 $I_{Mo}V_{Mo}$	I_3	5.6 I_{Mo}	8 V_{Mo}	44.8 $I_{Mo}V_{Mo}$	I_1	5.8 I_{Mo}	7 V_{Mo}	40.6 $I_{Mo}V_{Mo}$	I_3	5.8 I_{Mo}	8 V_{Mo}	46.4 $I_{Mo}V_{Mo}$
I_1	5.6 I_{Mo}	6 V_{Mo}	33.6 $I_{Mo}V_{Mo}$	I_8	5.6 I_{Mo}	8 V_{Mo}	44.8 $I_{Mo}V_{Mo}$	I_{10}	5.5 I_{Mo}	10 V_{Mo}	55 $I_{Mo}V_{Mo}$	I_1	5.8 I_{Mo}	6 V_{Mo}	34.8 $I_{Mo}V_{Mo}$	I_3	5.8 I_{Mo}	7 V_{Mo}	40.6 $I_{Mo}V_{Mo}$	I_4	5.8 I_{Mo}	8 V_{Mo}	46.4 $I_{Mo}V_{Mo}$
I_3	5.9 I_{Mo}	5 V_{Mo}	29.5 $I_{Mo}V_{Mo}$	I_4	5.8 I_{Mo}	5 V_{Mo}	29 $I_{Mo}V_{Mo}$	I_4	5.6 I_{Mo}	5 V_{Mo}	28 $I_{Mo}V_{Mo}$	I_4	5.8 I_{Mo}	6 V_{Mo}	34.8 $I_{Mo}V_{Mo}$	I_5	5.8 I_{Mo}	7 V_{Mo}	40.6 $I_{Mo}V_{Mo}$	I_6	5.8 I_{Mo}	8 V_{Mo}	46.4 $I_{Mo}V_{Mo}$
I_2	6 I_{Mo}	4 V_{Mo}	24 $I_{Mo}V_{Mo}$	I_7	6 I_{Mo}	4 V_{Mo}	24 $I_{Mo}V_{Mo}$	I_7	5.9 I_{Mo}	4 V_{Mo}	23.6 $I_{Mo}V_{Mo}$	I_6	5.8 I_{Mo}	6 V_{Mo}	34.8 $I_{Mo}V_{Mo}$	I_7	5.8 I_{Mo}	7 V_{Mo}	40.6 $I_{Mo}V_{Mo}$	I_8	5.8 I_{Mo}	8 V_{Mo}	46.4 $I_{Mo}V_{Mo}$
I_{10}	6.3 I_{Mo}	3 V_{Mo}	18.9 $I_{Mo}V_{Mo}$	I_9	6 I_{Mo}	4 V_{Mo}	24 $I_{Mo}V_{Mo}$	I_8	5.9 I_{Mo}	4 V_{Mo}	23.6 $I_{Mo}V_{Mo}$	I_9	5.8 I_{Mo}	6 V_{Mo}	34.8 $I_{Mo}V_{Mo}$	I_9	5.8 I_{Mo}	7 V_{Mo}	40.6 $I_{Mo}V_{Mo}$	I_9	5.8 I_{Mo}	8 V_{Mo}	46.4 $I_{Mo}V_{Mo}$
I_4	7.2 I_{Mo}	2 V_{Mo}	14.4 $I_{Mo}V_{Mo}$	I_{10}	6 I_{Mo}	4 V_{Mo}	24 $I_{Mo}V_{Mo}$	I_5	6 I_{Mo}	2 V_{Mo}	12 $I_{Mo}V_{Mo}$	I_7	6 I_{Mo}	2 V_{Mo}	12 $I_{Mo}V_{Mo}$	I_4	6.1 I_{Mo}	2 V_{Mo}	12.2 $I_{Mo}V_{Mo}$	I_{10}	5.8 I_{Mo}	8 V_{Mo}	46.4 $I_{Mo}V_{Mo}$
I_5	7.2 I_{Mo}	2 V_{Mo}	14.4 $I_{Mo}V_{Mo}$	I_3	6.3 I_{Mo}	1 V_{Mo}	6.3 $I_{Mo}V_{Mo}$	I_3	7 I_{Mo}	1 V_{Mo}	7 $I_{Mo}V_{Mo}$	I_{10}	6.5 I_{Mo}	1 V_{Mo}	6.5 $I_{Mo}V_{Mo}$	I_8	6.2 I_{Mo}	1 V_{Mo}	6.2 $I_{Mo}V_{Mo}$	I_7	6 I_{Mo}	1 V_{Mo}	6 $I_{Mo}V_{Mo}$

Where I_i is the ith row current, I_{Mo} is the module current at SOC.

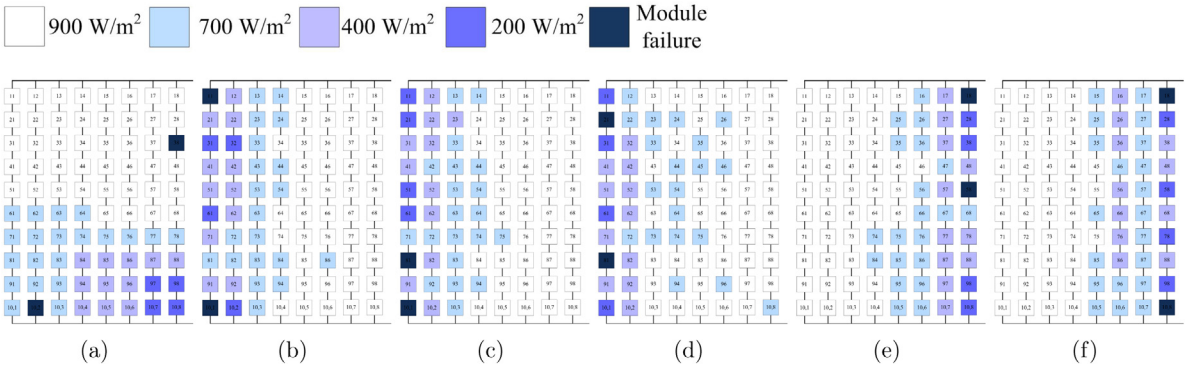

Fig. 4. The 9 × 9 PV array scheme in case of mismatch pattern 1 for (a) TCT without reconfiguration, (b) HHO, (c) MPA, (d) AEO, (e) HGS and (f) EHHGS.

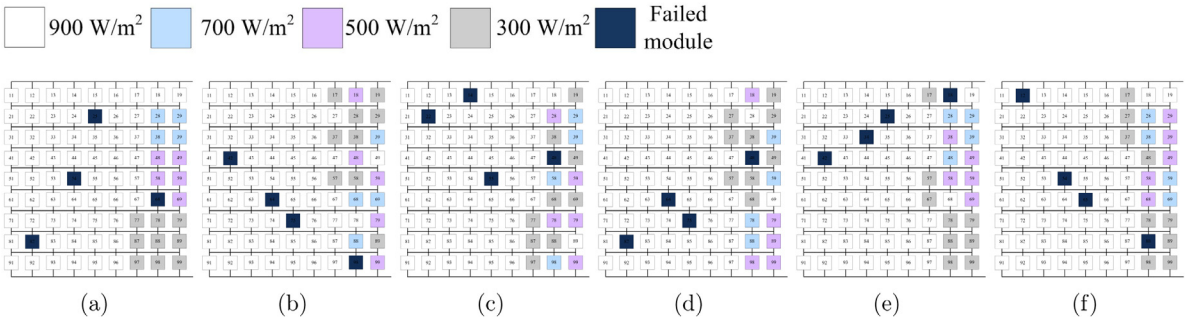

Fig. 5. The 9 × 9 PV array scheme in case of mismatch pattern 2 for (a) TCT without reconfiguration, (b) HHO, (c) MPA, (d) AEO, (e) HGS and (f) EHHGS.

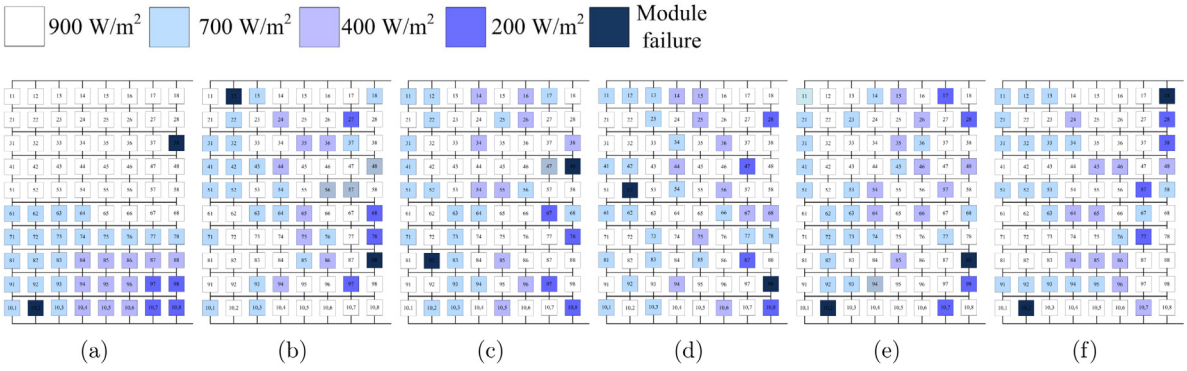

Fig. 6. The 10 × 8 PV array scheme in case of mismatch pattern 3 for (a) TCT without reconfiguration, (b) HHO, (c) MPA, (d) AEO, (e) HGS and (f) EHHGS.

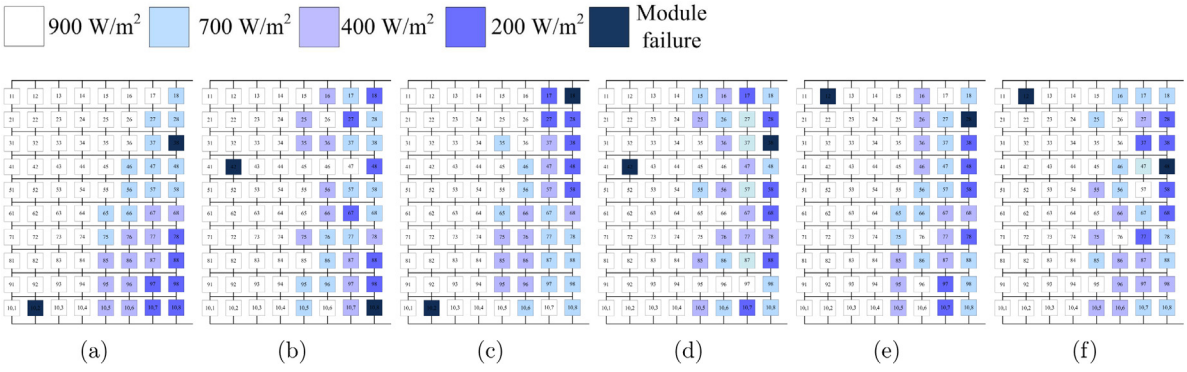

Fig. 7. The 10 × 8 PV array scheme in case of mismatch pattern 4 for (a) TCT without reconfiguration, (b) HHO, (c) MPA, (d) AEO, (e) HGS and (f) EHHGS.

For further assessment of the proposed EHHGS optimizer performance, four of the quality measurements are reported in Fig. 11 that are global maximum power Max_{power}, MPL, % PL, and % PH. The reported data illustrate the superiority of the

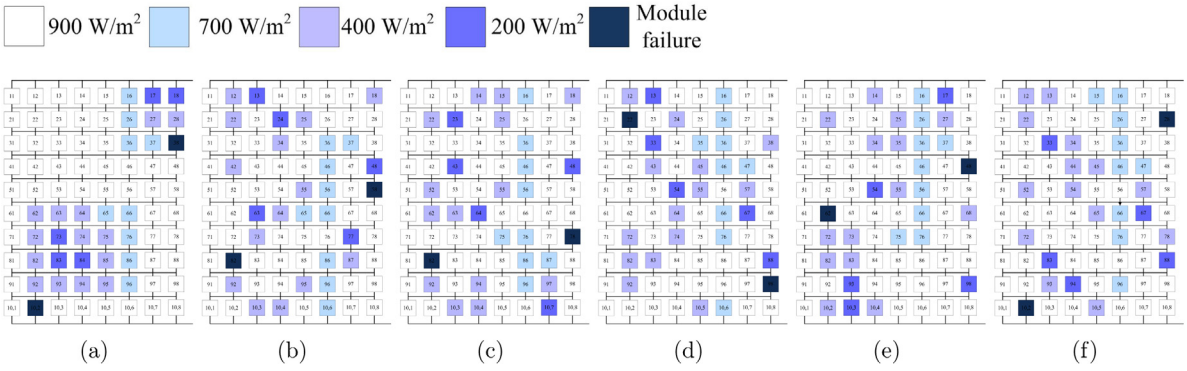

Fig. 8. The 10 × 8 PV array scheme in case of mismatch pattern 5 for (a) TCT without reconfiguration, (b) HHO, (c) MPA, (d) AEO, (e) HGS and (f) EHHGS.

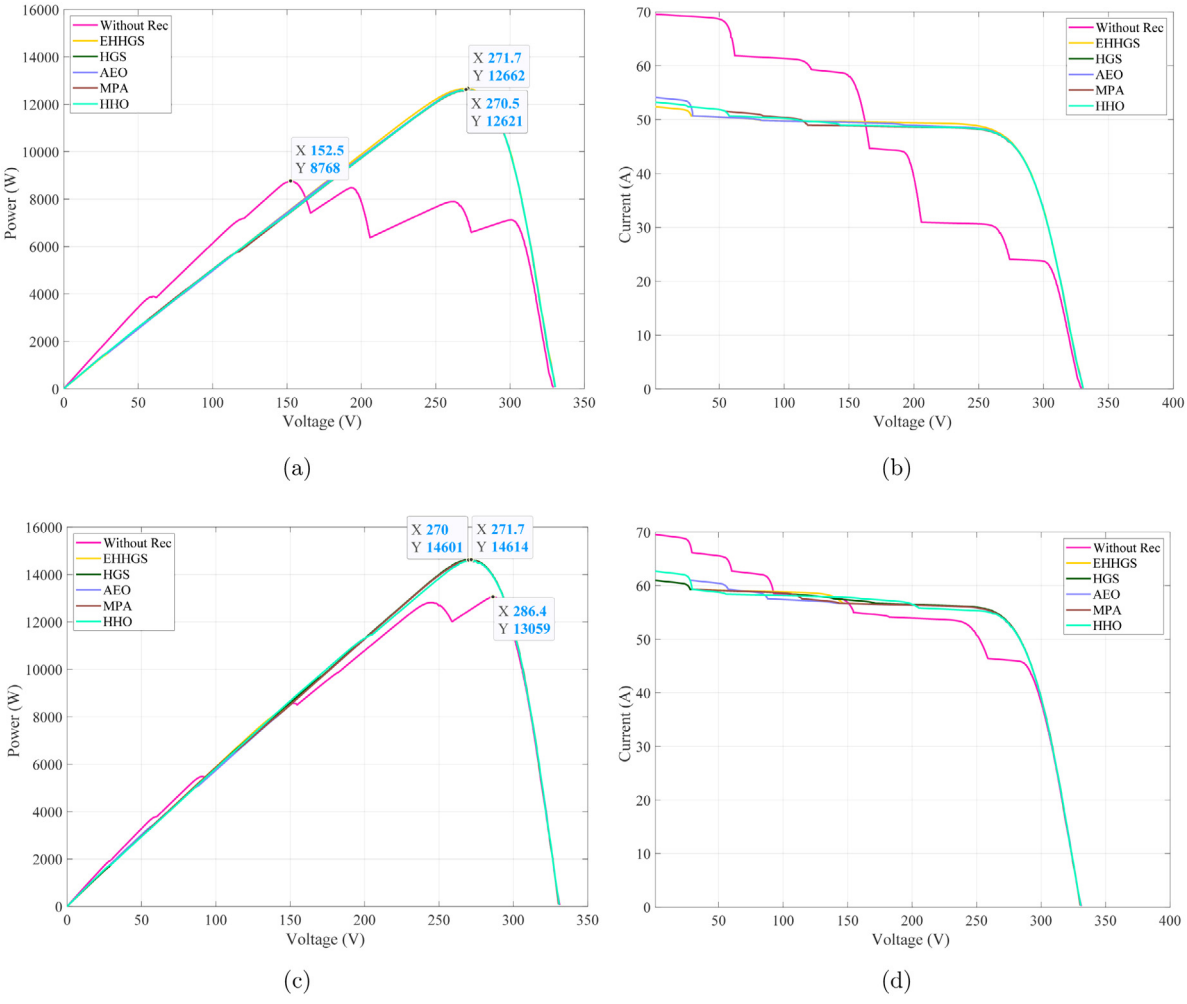

Fig. 9. The P–V and I–V characteristics of 9 × 9 PV array in the cases of (a) P–V Pattern 1, (b) I–V Pattern 1, and (c) P–V Pattern 2, (d) I–V Pattern 2 of TCT-connected PV arrays.

proposed EHHGS in providing more harvested power and minimizing the PL to 0.34799; meanwhile, the TCT without reconfiguration and other peers minimized the power loss by 0.54853, 0.35012, 0.35012, 0.35198, and 0.35116 as in pattern 1. Accordingly, the approach-based EHHGS enhanced the power generation by 44.4208%, 0.32753%, 0.32841%, 0.61562%, and 0.48811% compared with the TCT without reconfiguration, HGS, AEO, MPA, and HHO, respectively for pattern 1. Similarly, the results of the other patterns using the EHHGS optimizer provide a shred of evidence on the efficiency, robustness, and superiority of the optimizer in enhancing the produced PV power of the entire considered arrays.

To assess the consistency of the proposed optimizer statistically, a boxplot for the captured maximum power through the 30 separate tries by the EHHGS and other peers is plotted in Fig. 12. Furthermore, a pairwise unbiased comparison between the EHHGS and the other produced algorithms is achieved using the Wilcoxon signed-rank test with a significant difference of

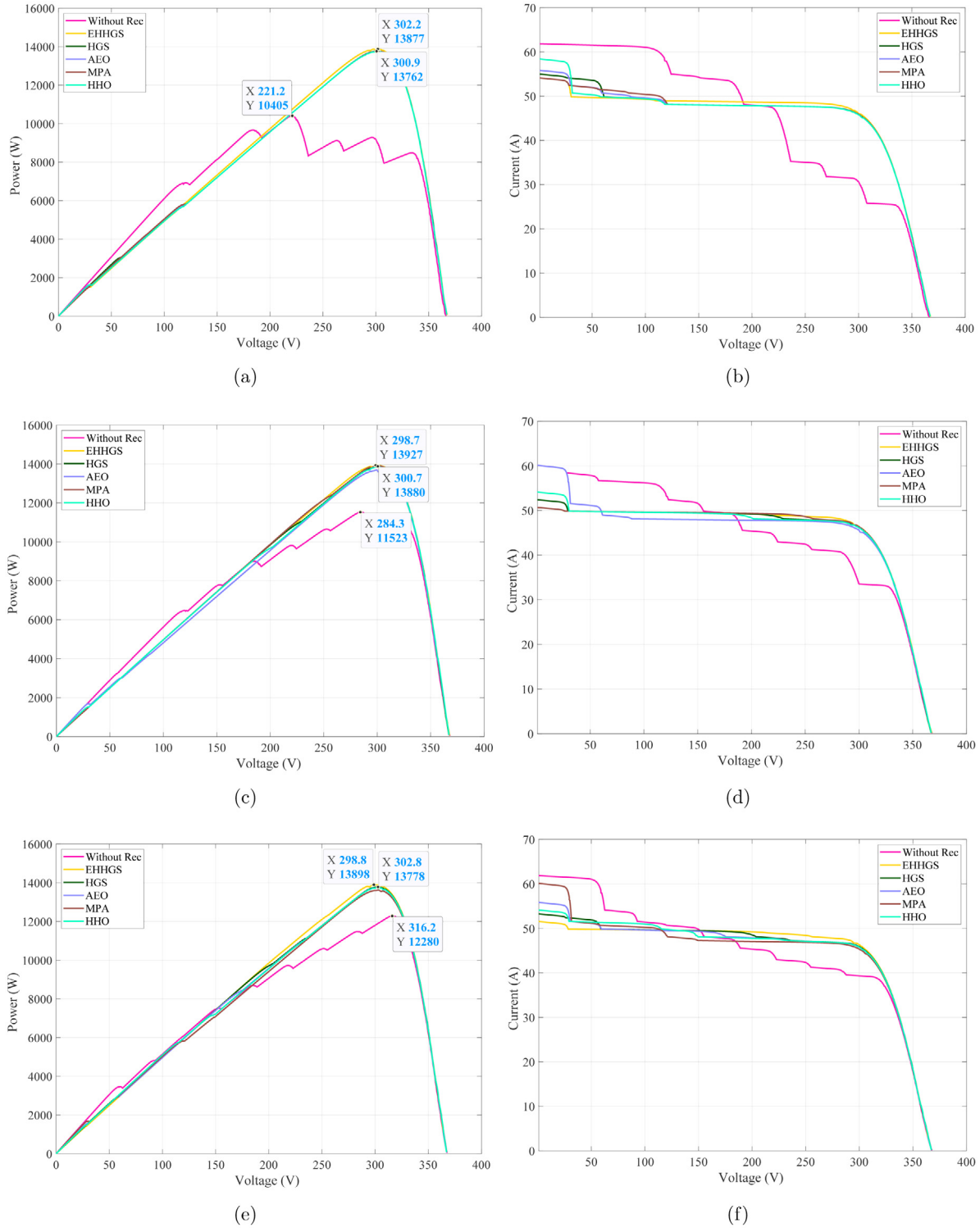

Fig. 10. The P–V and I–V characteristics of 10 × 8 PV array in the cases of (a) P–V Pattern 3, (b) I–V Pattern 3, (c) P–V Pattern 4, (d) I–V Pattern 4, (e) P–V Pattern 5, (f) I–V Pattern 5 of TCT-connected PV arrays.

0.05, as shown in Table 5. The test is performed based on the following strategy:

1. For the implemented methods, save the collected global power of the PV array over 30 separate runs based on the schemes of (EHHGS, HGS, AEO, MPA, and HHO).
2. Find the sum of ranks for runs in which the EHHGS has the best reaction (maximum power) as compared to other techniques such as HGS, AEO, MPA, and HHO (as determined by $R+$).
3. Find the sum of ranks for runs in which the HGS, AEO, MPA, or HHO has the peak power values in comparison to EHHGS (as indicated by $R-$).
4. Obtain the p-value in a statistical hypothesis test to see if the results are significantly different. The lower the p-value, the more evidence there is against the null

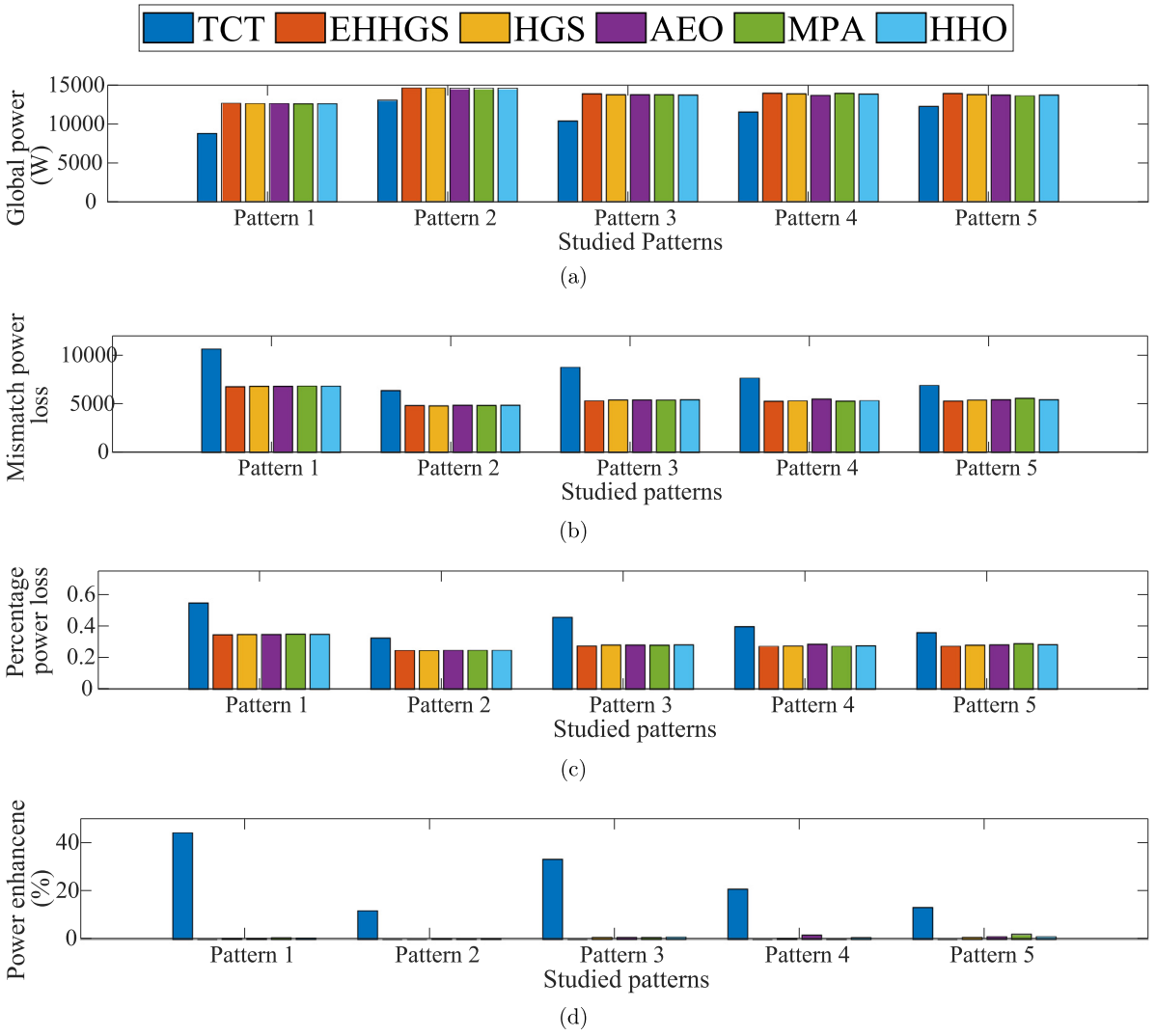

Fig. 11. Performance measures of EHHGS versus TCT, HGS and other peers for the considered TCT-interconnected PV arrays of (a) Max_{power} (W), (b) MPL (W), (c) PL, and (d) %PH of EHHGS versus TCT, MPA, HHO, AEO and HGS.

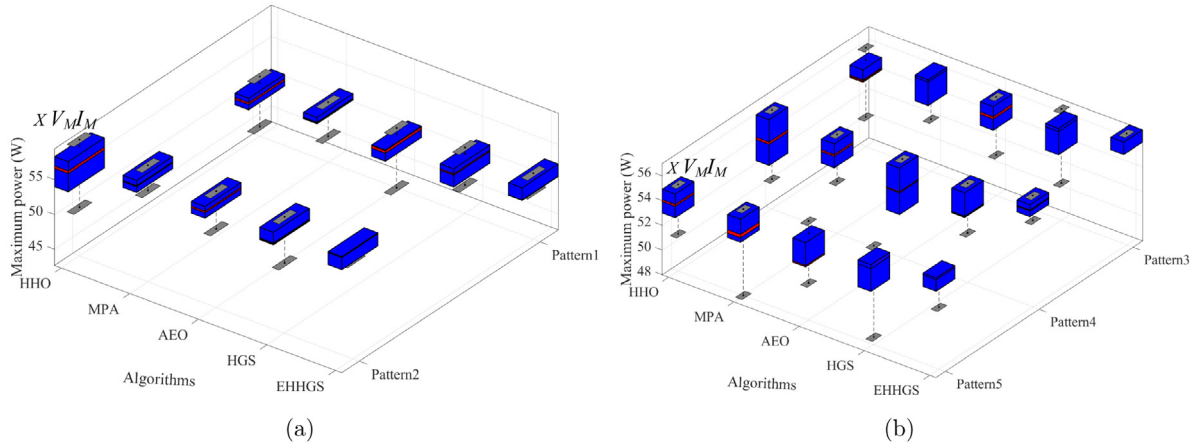

Fig. 12. The proposed EHHGS versus the counterparts performances from the point of the attained maximum power throughout 30 separate tries in cases of (a) 9 × 9 PV array, and (b) 10 × 8 connected S–P PV arrays.

hypothesis, indicating that there is significant variation between the approaches (p-value < 0.05). Then the null hypothesis ($H0$) is rejected. The term 'No' alludes to the rejection of the $H0$ in this work.

The plots of Fig. 12 illustrate the high consistency of the results of the EHHGS in comparison with the basic HGS and the other implemented techniques. The reported results in Table 5 show that the EHHGS has a significant difference in comparison with the

Table 5
Wilcoxon signed-rank non-parametric test of EHHGS vs HGS, or AEO, or MPA, HHO for the studied TCT-interconnected PV arrays.

Algs/metric		Patterns				
		Pattern 1	Pattern2	Pattern 3	Pattern 4	Pattern 5
EHHGS VS HGS	R_+	289.5	273	225.5	300	227
	R_-	61.5	52	5.5	0	26
	p-value	0.00344	0.00245	0.0001	0.00002	0.0009
	h_0	No	No	No	No	No
EHHGS VS AEO	R_+	273	112	325	325	370
	R_-	27	41	0	0	36
	p-value	0.00040	0.08869	0.00001	0.00001	0.00012
	h_0	No	yes	No	No	No
EHHGS VS MPA	R_+	237	145.5	231	344	267
	R_-	63	85.5	0	7	33
	p-value	0.01067	0.27913	0.00004	0.00001	0.00078
	h_0	No	yes	No	No	No
EHHGS VS HHO	R_+	292	358	351	344	308.5
	R_-	8	20	0	7	16.5
	p-value	0.0004	0.00005	0.00001	0.00002	0.00007
	h_0	No	No	No	No	No

compared peers as the p-values are less than 0.05. Furthermore, the R_+ and R_- values illustrate that the EHHGS accomplishes the most significant maximum power values throughout the number of separate trials compared to the HGS, AEO, and MPA and HHO ($R_+ > R_-$).

Finally, studying the mean execution time is one of the measurable factors, therefor bar-plots for the mean execution time of the EHHGS and other techniques are depicted in Fig. 13 for the 9×9 and 10×8 TCT interconnected PV arrays, respectively. Inspecting the figure shows that the execution time is considered the critical issue of the proposed EHHGS compared to the basic HGS; meanwhile, EHHGS consumes a time shorter than the other implemented algorithms (AEO, HHO, and MPA). Thus, the main finding is a trade-off between harvesting high power from the system with high consistency and waiting so some extra seconds in executions. Therefore, it is motivated to study the EHHGS convergence speed against its basic version of HGS, the convergence properties of the EHHGS versus the HGS are plotted in Fig. 14 in cases of distributing the shadow over 9×9 and 10×8 TCT interconnected PV arrays. The curves divulge the highly positive impact of the proposed modification on the basic HGS in boosting the exploration stage. Thus, the EHHGS can discover high-quality solutions faster than the HGS. By inspecting the curves, one can detect that the EHHGS converges to the maximum value of the fitness functions in the first number of iterations in contrast with the counterparts. Thus it is recommended for reconfiguring symmetric (9×9) and asymmetric (10×8) TCT-interconnected PV arrays. Then, however, the EHHGS has limitations in execution time compared with HGS, it provides the highest quality solutions that are reflected in the harvested power from the studied arrays in an earlier number of iterations. Thus, the fast convergence of the EHHGS is a solver for this limitation. Sequentially, the EHHS results have proven their superiority in consistency and providing the maximum levels of the PV output power over the studied patterns.

6.2. Series–parallel (S–P) connected system discussion

After evaluating the efficiency of the proposed EHHGS for tackling the reconfiguration process in TCT PV symmetric and asymmetric arrays. in this section, the SP PV arrays under five different patterns of shade considering random faulty modules are studied. The first and second patterns are applied on a PV array with of dimension of 9×9 while the other three patterns (3rd, 4th, *and* 5th) are considered for a 10×8 PV array. The distribution of shaded and random failed modules is described in the previous section of the TCT scheme as shown in Figs. 15(a), 16(a), 17(a), 18(a), and 19(a) for 9×9 and 10×8 S–P connection without reconfiguration.

The proposed EHHGS, HGS, HHO, MPA, and AEO are implemented to reconfigure the previously mentioned patterns to minimize mismatched power due to partial shading and random failures. The reconfigured arrays, as shown in Figs. 15, 16 for 9×9 PV array and in Figs. 17, 18, 19 for 10×8 PV array. The attained rearranged arrays by the EHHGS of Figs. 15(f), 16(f), 17(f), 18(f), and 19(f) show that the number of strings with shaded/failed modules in the reconfigured array is reduced compared with the S–P scheme without reconfiguration and schemes based on the counterparts (HGS, HHO, MPA, and AEO) for all evaluated cases. Furthermore, by inspecting the figures, it can be noticed that the failed modules which are sorely shaded are connected to the same string as many as possible when the proposed reconfiguration solution is adopted. Such structure can effectively improve the overall harvested power of the entire PV system.

The corresponded Power–Voltage (P–V) and Current–Voltage (I–V) characteristics to the patterns of Figs. 15–19 are depicted in Fig. 20 for 9×9 PV array and in Fig. 21 for 10×8 PV array. Inspecting the (P–V) curves while using the EHHGS-based rearrangement divulges the smoother curves with fewer local maximum power points (MPP) and higher values of the global MPP compared with the other curves. Furthermore, the curves of (I–V) characteristics reveal the efficiency of the obtained rearrangement by EHHGS in achieving more degradation in the curves compared with the other comparative schemes. This is an indicator of minimizing the mismatch losses effect while using the EHHGS-based schemes than the other strategies. Accordingly, it demonstrated that the proposed approach outperforms the other optimizers for all the studied patterns with more harvested power. For example, in pattern 1, the EHHGS-based scheme attains global maximum power Max_{power} of 11833.9264 W meanwhile the S–P scheme without reconfiguration shows MPP of 8037.7957 W accordingly the EHHGS enhanced the power by 47.2285% (see Fig. 20(a)). For the other counterparts (HHO, MPA, AEO, and HGS)-based schemes of pattern 1 of 9×9 PV array, the EHHGS-scheme can produce an additional power of 523.4074 W, 753.1103 W, 3315.8 W, and 1147.9 W, respectively. For the pattern 4 of 10×8 PV array, the EHHGS-based scheme provides an additional power generation of 3078.8 W, 808.6074 W, 642.5887 W, 864.5491 W, and 336.6097 W compared with S–P without reconfiguration, HHO, MPA, AEO, and HGD, respectively % (see Fig. 21(a)). Similar results can also be observed for the other patterns that approve the efficiency of the proposed approach.

For further analysis and investigation of the performance of the EHHGS approach, Fig. 22 presents a set of quality measures

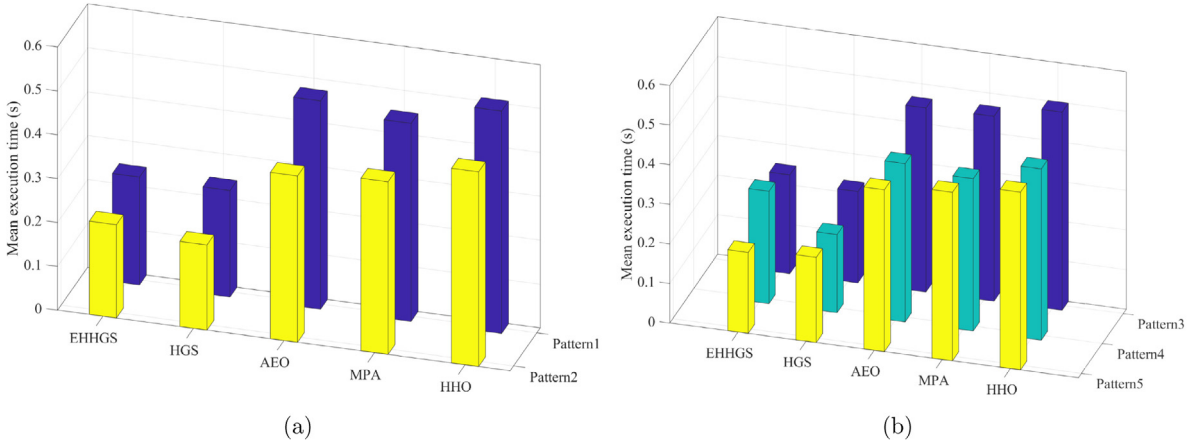

Fig. 13. The mean execution time throughout 30 separate tries of EHHGS versus the counterparts in cases of (a) 9 × 9 PV array, and (b) 10 × 8 connected TCT PV arrays.

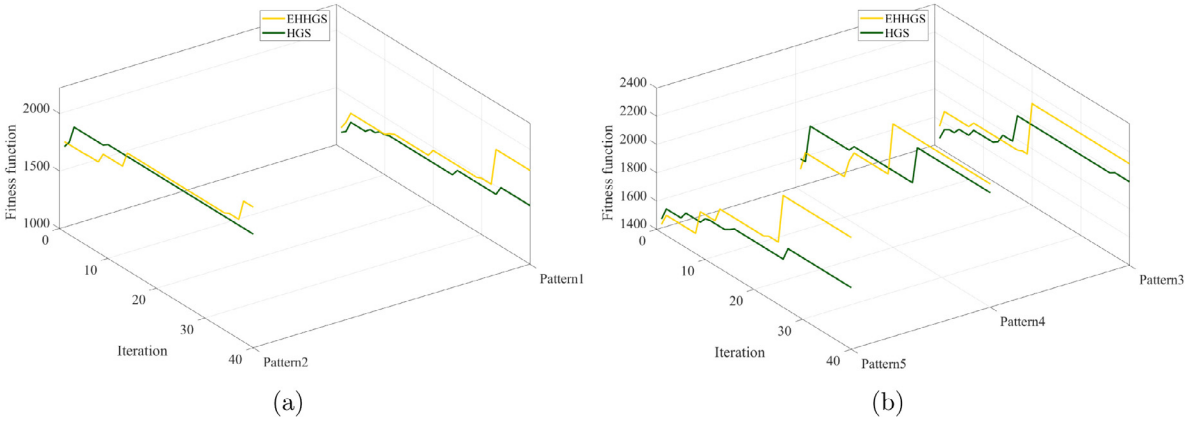

Fig. 14. The convergence property of the EHHGS versus the counterparts in cases of (a) 9 × 9 PV array, and (b) 10 × 8 connected TCT PV arrays.

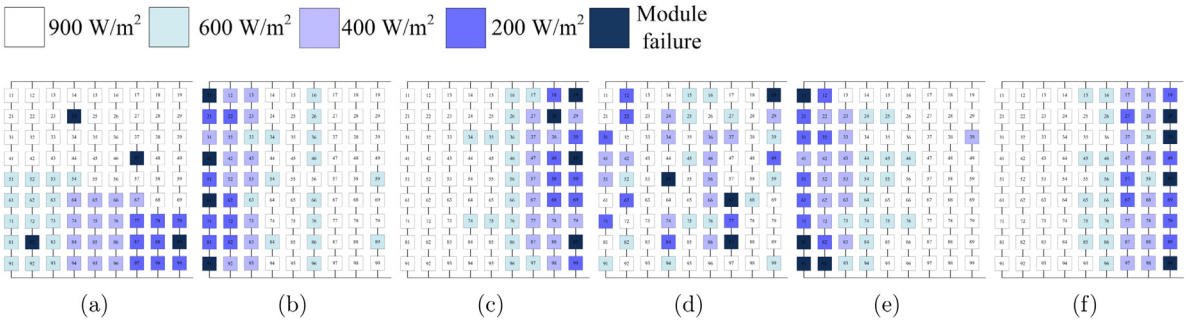

Fig. 15. The 9 × 9 PV array scheme in case of mismatch pattern 1 for (a) S–P without reconfiguration, (b) HHO, (c) MPA, (d) AEO, (e) HGS, and (f) EHHGS.

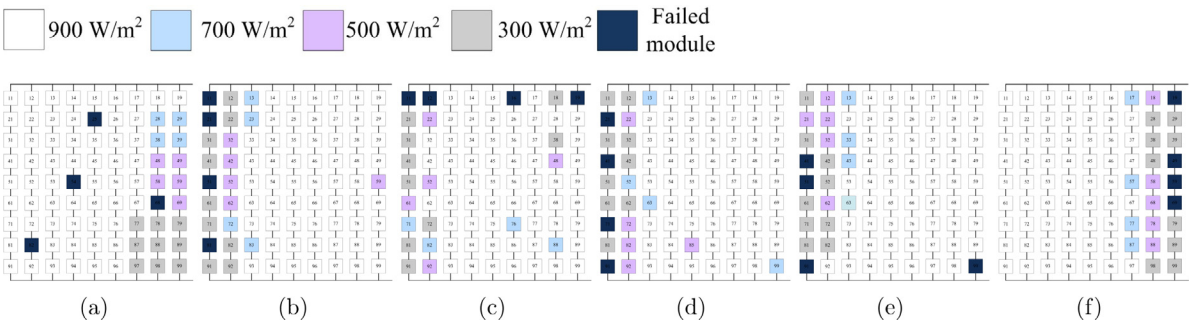

Fig. 16. The 9 × 9 PV array scheme in case of mismatch pattern 2 for (a) S–P without reconfiguration, (b) HHO, (c) MPA, (d) AEO, (e) HGS, and (f) EHHGS.

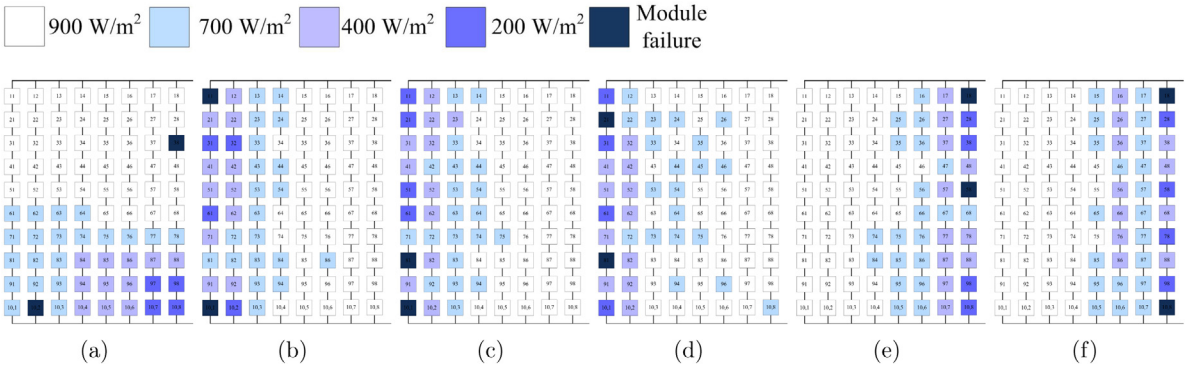

Fig. 17. The 10 × 8 PV array scheme in case of mismatch pattern 3 for (a) S–P without reconfiguration, (b) HHO, (c) MPA, (d) AEO, (e) HGS and (f) EHHGS.

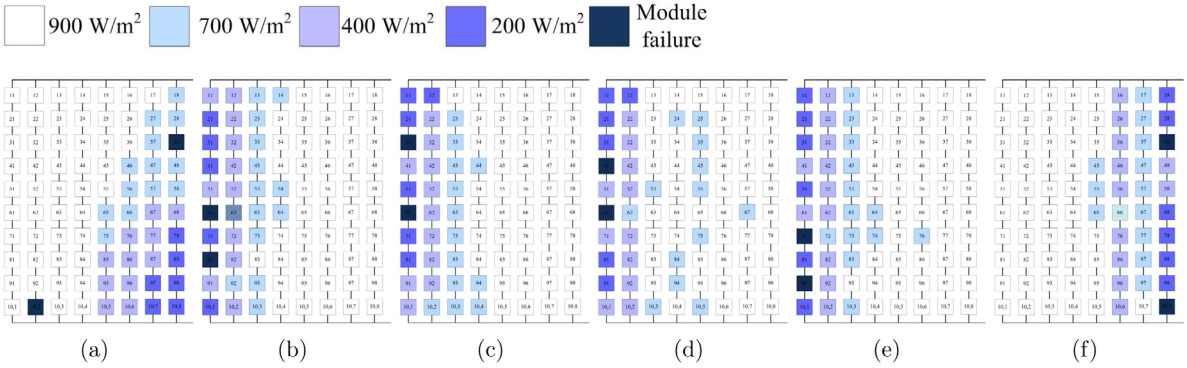

Fig. 18. The 10 × 8 PV array scheme in case of mismatch pattern 4 for (a) S–P without reconfiguration, (b) HHO, (c) MPA, (d) AEO, (e) HGS, and (f) EHHGS.

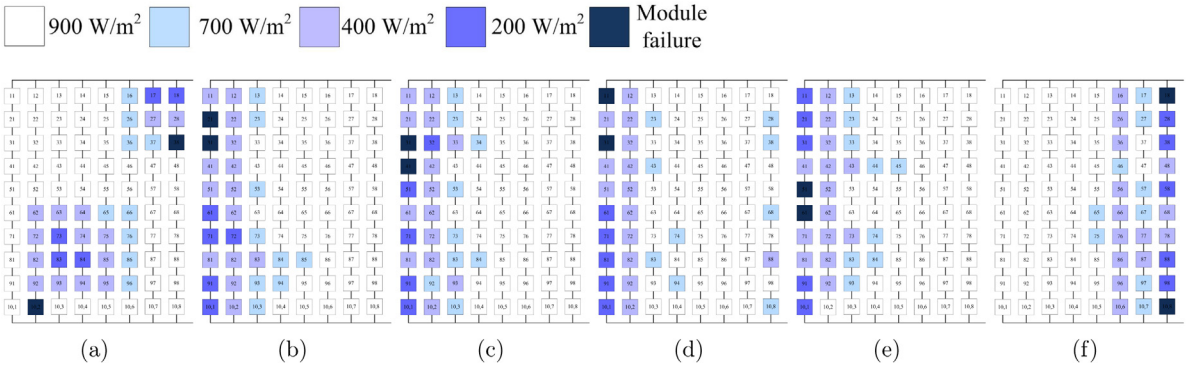

Fig. 19. The 10 × 8 PV array scheme in case of mismatch pattern 5 for (a) S–P without reconfiguration, (b) HHO, (c) MPA, (d) AEO, (e) HGS, and (f) EHHGS.

such as the obtained global maximum power values (Max_{power} (W)), MPL (W), % PL and % PH by EHHGS in comparison with the other peers. The results show that the proposed reconfigurations using EHHGS minimizes the MPL by 33.35%, 13.142%, 30.413%, 9.030%, and 6.4539% in comparison with S–P without reconfiguration, HGS, AEO, MPA, and HHO as in pattern 1. Moreover, the EHHGS approach enhances the harvested power by 47%, 10.7423%, 38.9267%, 6.7965%, and 4.6276% compared to the S–P without reconfiguration, HGS, AEO, MPA, and HHO in pattern 1, respectively. Similarly, the results affirm the superiority of the introduced methodology-based EHHGS throughout the studied patterns.

To provide an insight into the proposed EHHGS optimizer performance, its mean execution time is evaluated. Accordingly, bar plots for the mean execution time of the performed algorithms are plotted in Fig. 23 for 9 × 9 and 10 × 8 S–P interconnected PV arrays, respectively. The bars show the main limitation in the modified version is its higher execution time than the basic HGS, while it has a shorter time than HHO, AEO, and MPA thus EHHGS and HGS are the more comparable optimizers in the execution time. Sequentially, the convergence properties of the EHHGS versus HGS are plotted in Fig. 24 for cases of distributing the shadow over 9 × 9 and 10 × 8 S–P interconnected PV arrays. The curves divulge the highly positive impact of the proposed modification on the basic HGS in boosting the exploration stage. Thus, the EHHGS can discover high-quality solutions faster than the HGS. By inspecting the curves, one can detect that the EHHGS converges to the maximum value of the fitness functions in the first number of iterations in conversion with the HGS. Thus it is recommended for reconfiguring symmetric (9 × 9) and asymmetric (10 × 8) S–P-interconnected PV arrays.

Based on the previous discussions, one can conclude that the EHHGS has limitations in execution time compared with HGS. Meanwhile, EHHGS provides the highest quality solutions that are reflected in the harvested power from the studied arrays. Moreover, the fast convergence of the EHHGS is a solver for this

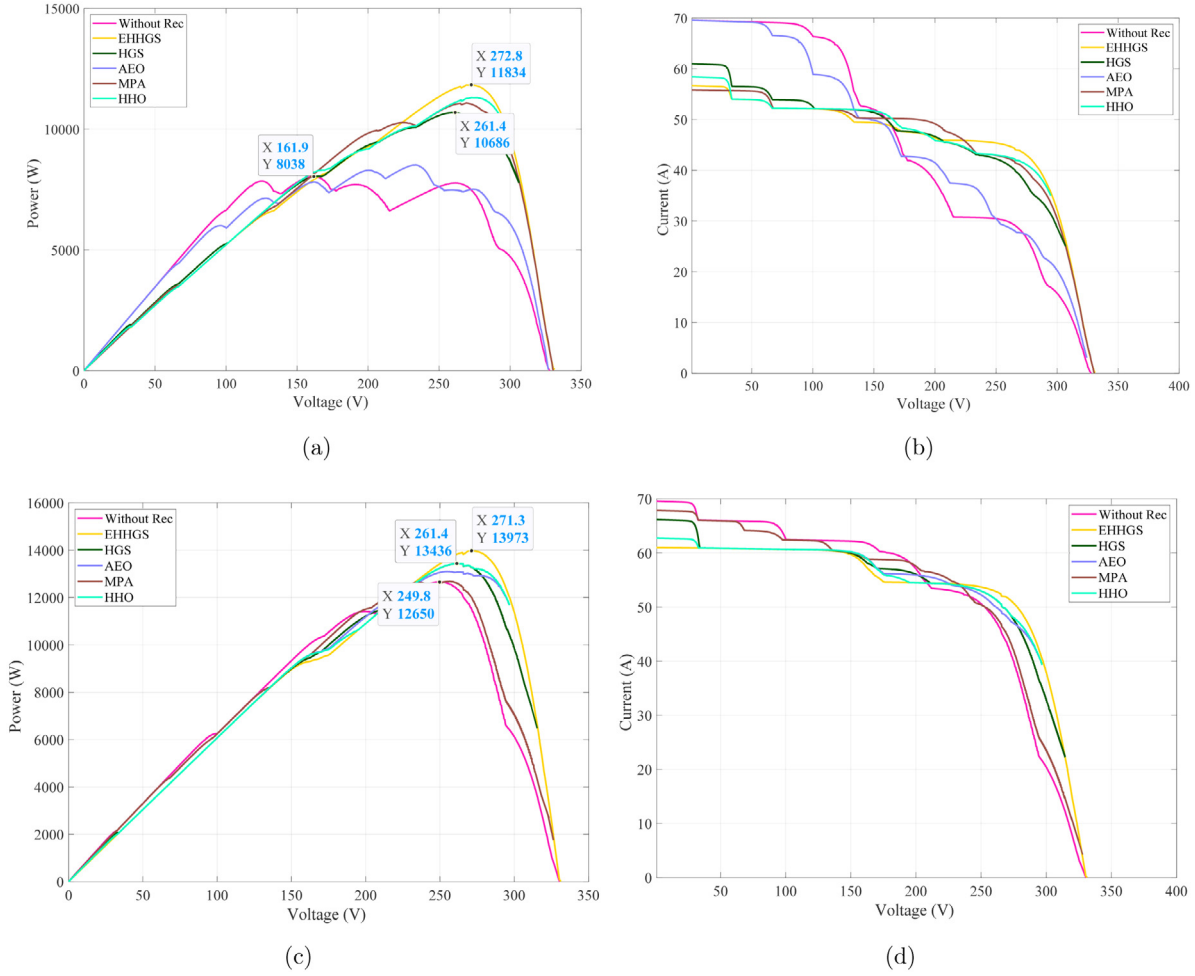

Fig. 20. The Power–Voltage (P–V) and Current–Voltage (I–V) characteristics of 9 × 9 of S–P-connected PV array in the cases of (a) P–V Pattern 1, (b) I–V Pattern 1, and (c) P–V Pattern 2, (d) I–V Pattern 2.

limitation as to the EHHGS cates the best solutions in the first number of iterations in contrast to the other peers and the basic HGS. That is why the EHHGS proves its efficiency in handling this optimization problem.

7. Conclusion

With the objective of providing a solution for the partial shading losses, reconfiguration is a method that greatly helps. Thereby in this article authors proposed an innovative reconfiguration technique via the novel Heterogeneous Hunger Games Search Optimizer (EHHGS) due to its various features.

The key findings of the work carried out in this article are exemplified as follows:

- A developed optimization algorithm of EHHGS has been proposed as an efficient tool for reconfiguring the TCT and S–P PV arrays under different operating conditions.
- A novel objective function is proposed by achieving maximum power, with the multiplication of the difference between the maximum and minimum power levels in the array and the average power across the array.
- The other innovation of the work is that the authors developed a graphical user interface (GUI) which helps the users/researchers to detect the performance of the entire PV array before and after the reconfiguration process. This GUI is a user-friendly system, by using this researchers can generate an optimal switching matrix under various scenarios. That is, researchers can choose different connection schemes, different array sizes, and different optimization algorithms. With the obtained switching matrix, the switching positions of the PV array can be changed to produce maximum power from the PV array. Based on the author's knowledge this is the first initiation to developing such a user-friendly GUI for the reconfiguration. In the future, this GUI can also be extended with various additional parameters to simplify the assessment.
- The proposed reconfiguration technique has been evaluated for two widely used connection schemes such as TCT and S–P with a PV array size of 10 × 8 and 9 × 9.
- Each PV connection scheme is tested with consideration of 5 different shade patterns and obtained results are tabulated.
- To assess the superiority of the proposed method, reconfiguration has been implemented by using other recent evolved optimization algorithms namely HHO, MPA, AEO, and HGS and obtained results are compared with various performance parameters.
- From the obtained results it is noteworthy to mention that, the proposed EHHGS exhibits superior performance, and maximum power generation and its also observed that, multiple peaks over P–V curves are minimized.
- From the carried out statistical analysis it is to highlight that, in the case of TCT connected system, EHHGS produces 44.42% and 11.9% of higher power than TCT connected system for 9 × 9 PV array under patterns 1 and 2. Likewise,

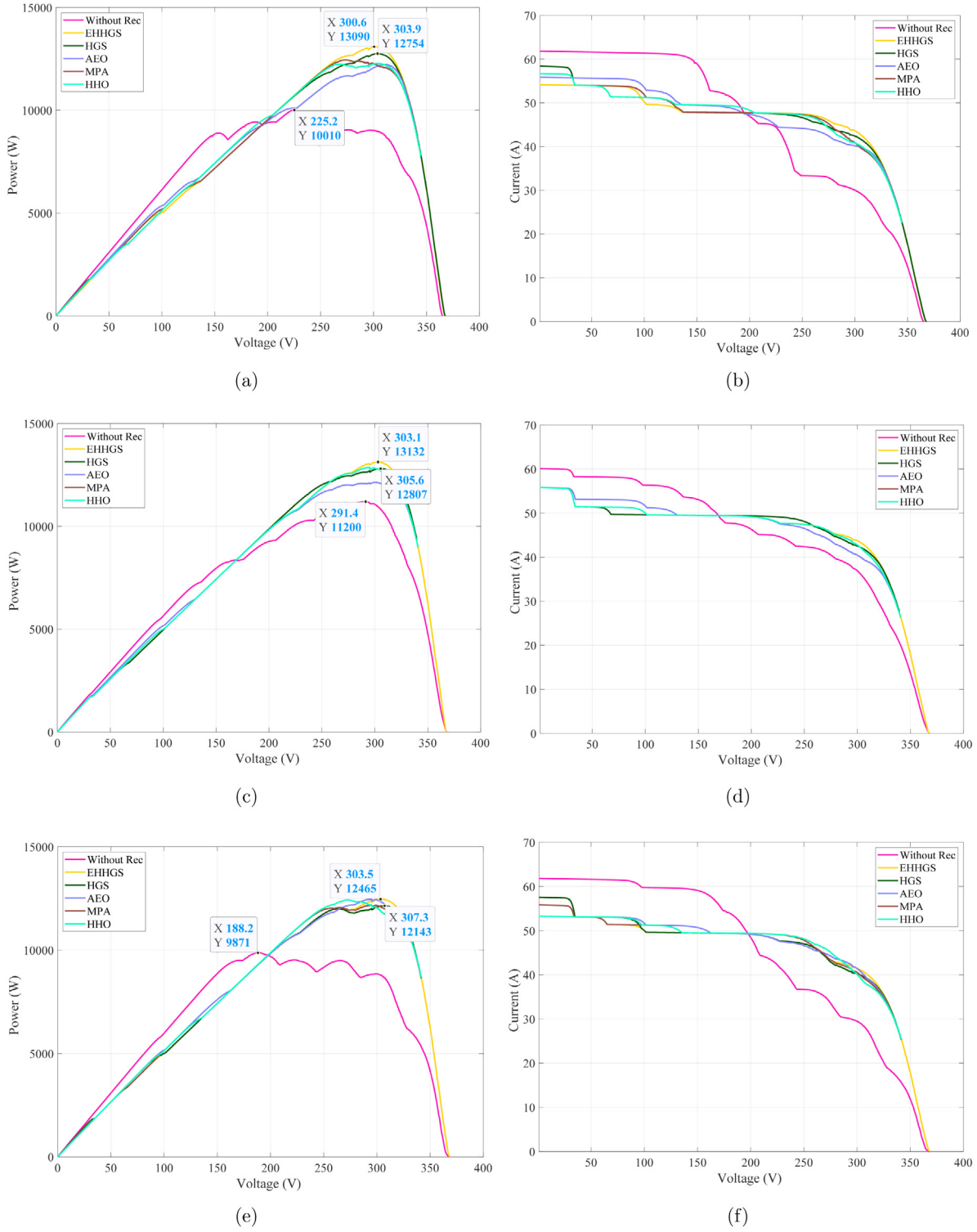

Fig. 21. The Power–Voltage (P–V) and Current–Voltage (I–V) characteristics of 10 × 8 of S–P-connected PV array in the cases of (a) P–V Pattern 3, (b) I–V Pattern 3, (c) P–V Pattern 4, (d) I–V Pattern 4, and (e) P–V Pattern 5, (f) I–V Pattern 5.

for 10 × 8 PV array the proposed EHHGS enhances power generation of 33.36%, 20.86%, 13.17% over TCT under shade pattern 3, 4, 5 respectively.

- Further, in the case of S–P connection the proposed EHHGS generates 47.2% and 10.45% higher power than S–P for array size of 9 × 9 under Pattern 1 and 2. Similarly, for 10 × 8 PV array, it produces enhanced power of 30.75%, 17.25%, and 26.27% under shade patter 3, 4, and 5.
- The convergence curves of the EHHGS are evidence of the favorable impact of the proposed modifications of dividing the agents into two separate groups for exploration and exploitation and enhancing the agents' motion with a nonlinear mutation operator.

With noticeable features, the EHHGS reconfiguration technique is found to be superior when compared with other counterparts and it acts as the best solution for the effect of partial shading.

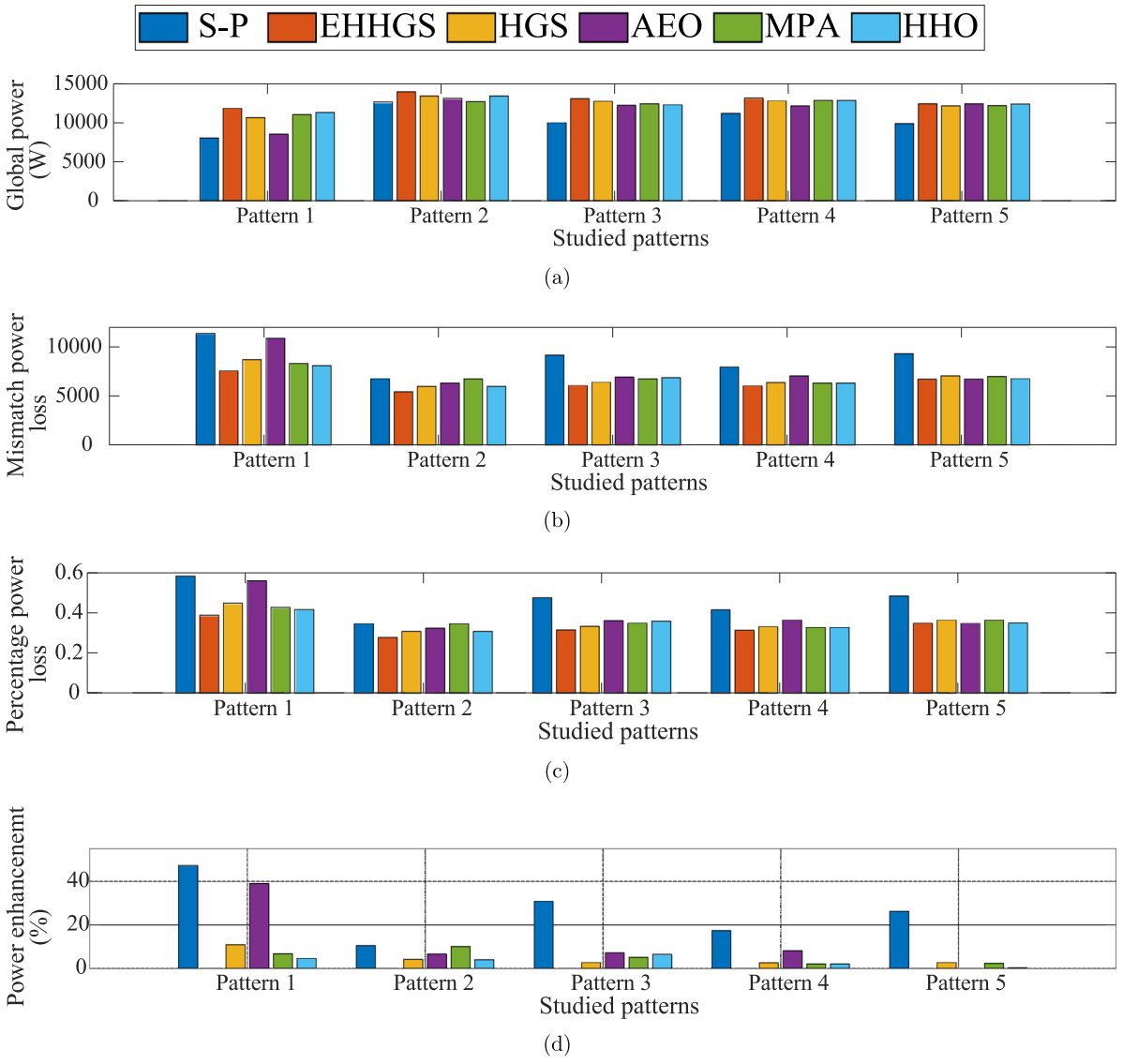

Fig. 22. Performance measures of EHHGS versus SP,HGS and other peers for the considered SP-interconnected PV arrays of (a) Max_{power} (W), (b) MPL (W), (c) PL, and (d) %PH of EHHGS versus S–P, MPA, HHO, AEO and HGS.

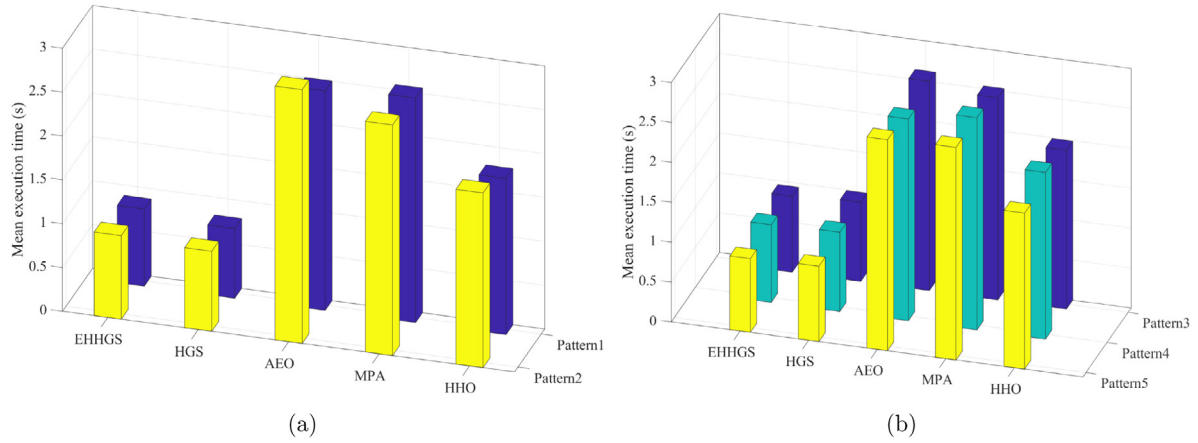

Fig. 23. The mean implementation time throughout 30 separate tries of EHHGS versus the counterparts in cases of (a) 9 × 9 PV array, and (b) 10 × 8 connected S–P PV arrays.

For future work, the proposed EHHGS will be applied to different applications to confirm its robustness. Moreover, the GUI tool will be generalized to involve several optimizers and configurations.

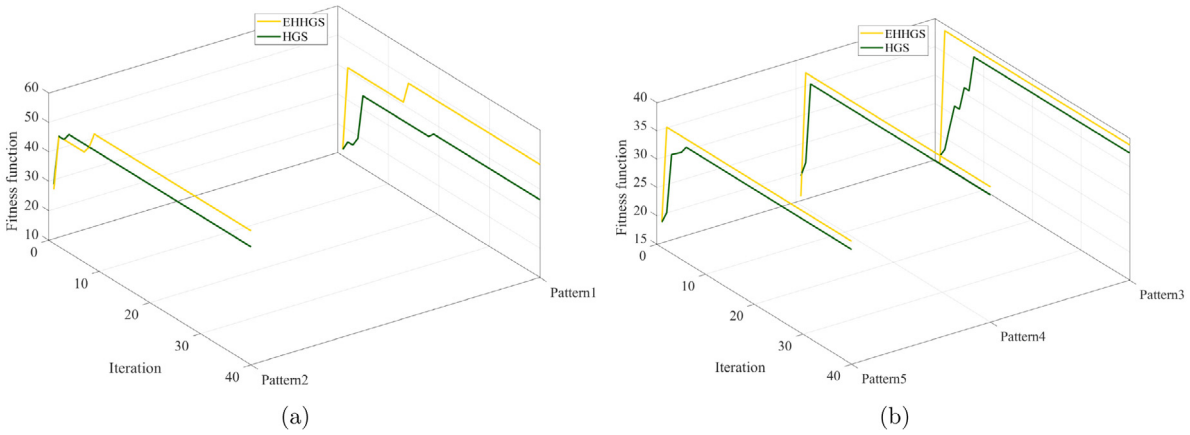

Fig. 24. The convergence property of the EHHGS versus the counterparts in cases of (a) 9 × 9 PV array, and (b) 10 × 8 connected S–P PV arrays.

Declaration of competing interest

The authors declare that they have no known competing financial interests or personal relationships that could have appeared to influence the work reported in this paper.

Data availability

Data will be made available on request.

Acknowledgments

This work is partially supported by CIRA-013-2020, Khalifa University, Abu Dhabi, United Arab Emirates.

References

Ajmal, A.M., Babu, T.S., Ramachandaramurthy, V.K., Yousri, D., Ekanayake, J.B., 2020. Static and dynamic reconfiguration approaches for mitigation of partial shading influence in photovoltaic arrays. Sustain. Energy Technol. Assess. 40, 100738.

Ajmal, A.M., Ramachandaramurthy, V.K., Naderipour, A., Ekanayake, J.B., 2021. Comparative analysis of two-step GA-based PV array reconfiguration technique and other reconfiguration techniques. Energy Convers. Manage. 230, 113806.

Akrami, M., Pourhossein, K., 2018. A novel reconfiguration procedure to extract maximum power from partially-shaded photovoltaic arrays. Sol. Energy 173, 110–119.

Alkahtani, M., Wu, Z., Kuka, C.S., Alahammad, M.S., Ni, K., 2020. A novel PV array reconfiguration algorithm approach to optimising power generation across non-uniformly aged PV arrays by merely repositioning. J.—Multidisciplinary Sci. J. 3 (1), 32–53.

Anon, 2003. Canadian solar CS6P-240P solar panels. https://www.siemen.co.uk/Sm55_sm50.html.

Babu, T.S., Ram, J.P., Dragičević, T., Miyatake, M., Blaabjerg, F., Rajasekar, N., 2017. Particle swarm optimization based solar PV array reconfiguration of the maximum power extraction under partial shading conditions. IEEE Trans. Sustain. Energy 9 (1), 74–85.

Babu, T.S., Yousri, D., Balasubramanian, K., 2020. Photovoltaic array reconfiguration system for maximizing the harvested power using population-based algorithms. IEEE Access 8, 109608–109624.

Deshkar, S.N., Dhale, S.B., Mukherjee, J.S., Babu, T.S., Rajasekar, N., 2015. Solar PV array reconfiguration under partial shading conditions for maximum power extraction using genetic algorithm. Renew. Sustain. Energy Rev. 43, 102–110.

Dhanalakshmi, B., Rajasekar, N., 2018. A novel competence square based PV array reconfiguration technique for solar PV maximum power extraction. Energy Convers. Manage. 174, 897–912.

El-Dein, M.S., Kazerani, M., Salama, M., 2012. Optimal photovoltaic array reconfiguration to reduce partial shading losses. IEEE Trans. Sustain. Energy 4 (1), 145–153.

Faldella, E., Cardinali, G.C., Calzolari, P.U., 1991. Architectural and design issues on optimal management of photovoltaic pumping systems. IEEE Trans. Ind. Electron. 38 (5), 385–392.

Fang, X., Yang, Q., Yan, W., 2021. Switching matrix enabled optimal topology reconfiguration for maximizing power generation in series–parallel organized photovoltaic systems. IEEE Syst. J..

Fathy, A., 2018. Recent meta-heuristic grasshopper optimization algorithm for optimal reconfiguration of partially shaded PV array. Sol. Energy 171, 638–651.

Fathy, A., 2020. Butterfly optimization algorithm based methodology for enhancing the shaded photovoltaic array extracted power via reconfiguration process. Energy Convers. Manage. 220, 113115.

Krishna, G.S., Moger, T., 2019a. Improved SuDoKu reconfiguration technique for total-cross-tied PV array to enhance maximum power under partial shading conditions. Renew. Sustain. Energy Rev. 109, 333–348.

Krishna, G.S., Moger, T., 2019b. Reconfiguration strategies for reducing partial shading effects in photovoltaic arrays: State of the art. Sol. Energy 182, 429–452.

Krishna, G.S., Moger, T., 2021. A novel adaptive dynamic photovoltaic reconfiguration system to mitigate mismatch effects. Renew. Sustain. Energy Rev. 141, 110754.

La Manna, D., Vigni, V.L., Sanseverino, E.R., Di Dio, V., Romano, P., 2014. Reconfigurable electrical interconnection strategies for photovoltaic arrays: A review. Renew. Sustain. Energy Rev. 33, 412–426.

Lim, L.H.I., Ye, Z., Ye, J., Yang, D., Du, H., 2015. A linear identification of diode models from single *I–V* characteristics of PV panels. IEEE Trans. Ind. Electron. 62 (7), 4181–4193.

Lowe, R., Drummond, P., 2022. Solar, wind and logistic substitution in global energy supply to 2050 – Barriers and implications. Renew. Sustain. Energy Rev. 153 (6), 111720.

Malathy, S., Ramaprabha, R., 2018. Reconfiguration strategies to extract maximum power from photovoltaic array under partially shaded conditions. Renew. Sustain. Energy Rev. 81, 2922–2934.

Meerimatha, G., Rao, B.L., 2020. Novel reconfiguration approach to reduce line losses of the photovoltaic array under various shading conditions. Energy 196, 117120.

Mehedi, I., Salam, Z., Ramli, M., Chin, V., Bassi, H., Rawa, M., Abdullah, M., 2021. Critical evaluation and review of partial shading mitigation methods for grid-connected PV system using hardware solutions: The module-level and array-level approaches. Renew. Sustain. Energy Rev. 146, 111138.

Murugesan, P., David, P.W., Balachandran, P.K., Kumar, C.S., Babu, T.S., Alhelou, H.H., 2021. A new Ken-Ken puzzle pattern based reconfiguration technique for maximum power extraction in partial shaded solar PV array. IEEE Access.

Nahidan, M.H., Niroomand, M., Dehkordi, B.M., 2021. Power enhancement under partial shading condition using a two-step optimal PV array reconfiguration. Int. J. Photoenergy 2021.

Nazeri, M.N.R., Tajuddin, M.F.N., Babu, T.S., Azmi, A., Malvoni, M., Kumar, N.M., 2021. Firefly algorithm-based photovoltaic array reconfiguration for maximum power extraction during mismatch conditions. Sustainability 13 (6), 3206.

Ngoc, T.N., Phung, Q.N., Tung, L.N., Sanseverino, E.R., Romano, P., Viola, F., 2017. Increasing efficiency of photovoltaic systems under non-homogeneous solar irradiation using improved dynamic programming methods. Sol. Energy 150, 325–334.

Nihanth, M.S.S., Ram, J.P., Pillai, D.S., Ghias, A.M., Garg, A., Rajasekar, N., 2019. Enhanced power production in PV arrays using a new skyscraper puzzle based one-time reconfiguration procedure under partial shade conditions (PSCs). Sol. Energy 194, 209–224.

Nishioka, K., Sakitani, N., Uraoka, Y., Fuyuki, T., 2007. Analysis of multicrystalline silicon solar cells by modified 3-diode equivalent circuit model taking leakage current through periphery into consideration. Sol. Energy Mater. Sol. Cells 91 (13), 1222–1227.

Pachauri, R., Singh, R., Gehlot, A., Samakaria, R., Choudhury, S., 2019. Experimental analysis to extract maximum power from PV array reconfiguration under partial shading conditions. Eng. Sci. Technol. Int. J. 22 (1), 109–130.

Premkumar, M., Subramaniam, U., Babu, T.S., Elavarasan, R.M., Mihet-Popa, L., 2020. Evaluation of mathematical model to characterize the performance of conventional and hybrid PV array topologies under static and dynamic shading patterns. Energies 13 (12), 3216.

Rakesh, N., Madhavaram, T.V., 2016. Performance enhancement of partially shaded solar PV array using novel shade dispersion technique. Front. Energy 10 (2), 227–239.

Ramasamy, S., Seenithangam, J., Dash, S.S., Chaitanya, K., 2016. A dodging algorithm to reconfigure photovoltaic array to negate partial shading effect. Prog. Photovolt., Res. Appl. 24 (2), 200–210.

Rezk, H., Fathy, A., Aly, M., 2021. A robust photovoltaic array reconfiguration strategy based on coyote optimization algorithm for enhancing the extracted power under partial shadow condition. Energy Rep. 7, 109–124.

Salameh, Z.M., Dagher, F., 1990. The effect of electrical array reconfiguration on the performance of a PV-powered volumetric water pump. IEEE Trans. Energy Convers. 5 (4), 653–658.

Satpathy, P.R., Sharma, R., 2018. Power loss reduction in partially shaded PV arrays by a static SDP technique. Energy 156, 569–585.

Satpathy, P.R., Sharma, R., 2019. Power and mismatch losses mitigation by a fixed electrical reconfiguration technique for partially shaded photovoltaic arrays. Energy Convers. Manage. 192, 52–70.

Srinivasan, A., Devakirubakaran, S., Sundaram, B.M., 2020. Mitigation of mismatch losses in solar PV system–two-step reconfiguration approach. Sol. Energy 206, 640–654.

Trindade, F.C., Ferreira, T.S., Lopes, M.G., Freitas, W., 2016. Mitigation of fast voltage variations during cloud transients in distribution systems with PV solar farms. IEEE Trans. Power Deliv. 32 (2), 921–932.

Varma, G.H.K., Barry, V.R., Jain, R.K., Kumar, D., 2021. An MMTES algorithm for dynamic photovoltaic array reconfiguration to enhance power output under partial shading conditions. IET Renew. Power Gener. 15 (4), 809–820.

Venkateswari, R., Rajasekar, N., 2020. Power enhancement of PV system via physical array reconfiguration based lo shu technique. Energy Convers. Manage. 215, 112885.

Wang, S., Liu, G., Gao, M., Cao, S., Guo, A., Wang, J., 2020. Heterogeneous comprehensive learning and dynamic multi-swarm particle swarm optimizer with two mutation operators. Inform. Sci. 540, 175–201.

Yadav, K., Kumar, B., Swaroop, D., 2020. Mitigation of mismatch power losses of PV array under partial shading condition using novel odd even configuration. Energy Rep. 6, 427–437.

Yang, Y., Chen, H., Heidari, A.A., Gandomi, A.H., 2021. Hunger games search: Visions, conception, implementation, deep analysis, perspectives, and towards performance shifts. Expert Syst. Appl. 177, 114864.

Yousri, D., Allam, D., Eteiba, M.B., 2020a. Optimal photovoltaic array reconfiguration for alleviating the partial shading influence based on a modified harris hawks optimizer. Energy Convers. Manage. 206, 112470.

Yousri, D., Babu, T.S., Beshr, E., Eteiba, M.B., Allam, D., 2020b. A robust strategy based on marine predators algorithm for large scale photovoltaic array reconfiguration to mitigate the partial shading effect on the performance of PV system. IEEE Access 8, 112407–112426.

Yousri, D., Babu, T.S., Mirjalili, S., Rajasekar, N., Abd Elaziz, M., 2020c. A novel objective function with artificial ecosystem-based optimization for relieving the mismatching power loss of large-scale photovoltaic array. Energy Convers. Manage. 225, 113385.

Yousri, D., Thanikanti, S.B., Allam, D., Ramachandaramurthy, V.K., Eteiba, M., 2020d. Fractional chaotic ensemble particle swarm optimizer for identifying the single, double, and three diode photovoltaic models' parameters. Energy 195, 116979.

Yousri, D., Thanikanti, S.B., Balasubramanian, K., Osama, A., Fathy, A., 2020e. Multi-objective grey wolf optimizer for optimal design of switching matrix for shaded PV array dynamic reconfiguration. IEEE Access 8, 159931–159946.

Zhu, Z., Hou, M., Ding, L., Zhu, G., Jin, Z., 2020. Optimal photovoltaic array dynamic reconfiguration strategy based on direct power evaluation. IEEE Access 8, 210267–210276.